Isoprene production in seawater of Funka Bay, Hokkaido, Japan

Atsushi Ooki*, Ryuta Shida, Masashi Otsu, Hiroji Onishi, Naoto Kobayashi, Takahiro Iida, Daiki Nomura, Kota Suzuki, Hideyoshi Yamaoka, and Tetsuya Takatsu

Faculty of Fisheries Sciences, Hokkaido University, 3-1-1 Minato, Hakodate, Hokkaido 041-8611, Japan

*Corresponding Author: Atsushi Ooki
3-1-1 Minato, Hakodate, Hokkaido 041-8611, Japan
Tel: +81-138-40-8870; E-mail: ooki@fish.hokudai.ac.jp

Short title: Isoprene production in Funka Bay

Key words: Volatile organic compound (VOC), phytoplankton, bloom, photosynthesis, dark production, C_5H_8, hydrocarbon

Abstract (less than 250 words)

We carried out shipboard observations in Funka Bay, Hokkaido, Japan, monthly or bimonthly from December 2015 to November 2016. We measured vertical profiles of isoprene, chlorophyll-a (chl-a), and other parameters from surface to bottom layer (about 95 m) near the center of the bay. We found substantial increases in isoprene concentration in the surface mixed layer from February to March during the peak of the spring diatom bloom, in the bottom layer from March to April after the peak of the bloom, and in the subsurface layer (below the surface mixed layer) in summer from July to August, where there were also substantial chl-a concentration maxima. We attribute the isoprene increases in the surface and subsurface layers to photosynthetic production of isoprene by the dominant phytoplankton in the spring bloom and in summer, and that in the bottom layer to dark production of isoprene by diatom aggregates that settled from the surface euphotic zone. We also measured isoprene production in laboratory incubation experiments. The in-situ production rates of isoprene per unit chl-a in the surface mixed layer in the spring bloom, in the dark bottom layer during the bloom, and in the subsurface layer in summer (0.82, 0.03–0.13, and 7.38 pmol (μg chl-a)$^{-1}$ d^{-1}, respectively) were consistent with our incubation results. We believe that this is the first report focused on dark production of isoprene by diatoms; the production rate of isoprene under the dark condition ranged from 4% up to 16% of that by photosynthesis.

1. Introduction

Isoprene (2-methyl-1,3-butadiene; C_5H_8) comprises about half of the total global biogenic volatile organic compound (BVOC) emissions of 1 Pg (Guenther et al. 2012). Isoprene influences the oxidation capacity of the air by reacting with hydroxyl radicals (OH^-), nitrate radicals (NO_3), and ozone (O_3) (Lelieveld et al. 2008). Although terrestrial vegetation accounts for the largest emissions of isoprene, marine-derived isoprene can also influence the oxidation capacity of remote marine air because the lifetime of isoprene in marine air (several hours) is much less than the transport time (several days) from terrestrial sources to remote regions of the ocean (Broadgate et al. 1997; Palmer and Shaw 2005).

Marine isoprene is thought to be directly emitted from marine phytoplankton (e.g. Dani et al. 2017) and macroalgae (e.g. Broadgate et al. 2004) in association with their photosynthesis. A depth profile of isoprene concentration in the Gulf Stream off the Florida coast is similar to that of biological productivity as indicated by chl-a fluorescence (Milne et al. 1995). A global map of isoprene distribution obtained from some snap-shot observations (Ooki et al. 2015) shows high concentrations of isoprene (75–165 pmol L^{-1}) localized in subtropical–subarctic transitional waters of shelf and slope areas in the western northwest Pacific Ocean near Japan in high productive season, where there was a spring phytoplankton bloom and chl-a concentrations were notably high (4.1–10.3 μg L^{-1}).

High correlations between marine isoprene and chl-a have been reported in many studies; for example in the northwest Pacific Ocean near Japan (Kurihara et al. 2010), Sagami Bay, Japan (Kurihara et al. 2012) and the East China Sea (Li et al. 2018). Isoprene production rates per unit chlorophyll (mol [g chl-a]$^{-1}$ d^{-1}) by phytoplankton were measured in a number of incubation experiments, as summarized in Table 2 of Shaw et al. (2010), ranging over two orders of magnitude, depending on phytoplankton species and light intensity.

Isoprene production rates have been previously calculated from the measured isoprene concentrations in the surface mixed layer of the ocean basins (southeastern Pacific and southern Indian oceans) by three snap-shot observations assuming a steady state for isoprene in the mixed layer (Booge et al. 2018). The spatial variation of isoprene production rates was influenced by temperature, light intensity, nutrient levels, and salinity, which are also important factors for determining the plankton community and productivity. The steady-state assumption would be appropriate for calculating the spatial distribution of isoprene production on a basin scale; however, the isoprene concentrations vary widely with time. For example, the isoprene concentrations in the surface mixed layer doubled in 10 days within an iron-fertilized patch, where the phytoplankton cell numbers showed 4- to 20-fold increases over the same period (Moore and Wang 2006). The isoprene concentrations obviously respond to phytoplankton growth within several days.

Arnold et al. (2009) have evaluated the global ocean as an isoprene source by combining isoprene production rates of several phytoplankton types measured in laboratory incubations, satellite datasets of ocean biology, field observation datasets, and a global atmospheric chemistry model. They recommended that the combination of laboratory-measured individual phytoplankton isoprene productivities should be compared with true community isoprene productivities obtained from field observations. Therefore, isoprene production rate by a natural biological community should be evaluated within an identical water mass by time-series observation conducted in a semi-closed ocean area, such as semi-closed bay.

Many of previous studies focused on photosynthetic production of isoprene by plants, however, it has been reported that isoprene can also be formed by higher plants via the breakdown of stored carbohydrates when photosynthesis is blocked (Lerdau et al. 1997). It has been reported that the dark release of isoprene occurs in cells of all living organisms (Sanadze, 2004). A dark release of isoprene by marine organisms has not

been mentioned so far, it is possible that the dark releases by marine organisms including micro algae can increase the isoprene concentration in seawater. As for isoprene consumption, several studies have reported that the soil provides a sink for atmospheric isoprene due to consumptions by microorganisms in the soil (Cleveland and Yavitt, 1998), and that the ubiquitous marine hydrocarbon-degrader, Alcanivorax borkumensis, can degrade isoprene in seawater (Alvarez et al., 2009). The turnover time of isoprene by chemical loss, mainly reaction with OH, has been estimated to be 19 days which is much shorter (< 10%) than timescale of the biological production rate (Palmer and Shaw, 2005). Therefore, we have to notice that the isoprene production in a natural biological community is a net production including biological and chemical degradations as well as biological productions.

The purpose of this study was to estimate in-situ production rates of isoprene in a natural biological community from time-series observations in Funka Bay, Hokkaido, Japan. The observed in-situ production rates were compared with the rates measured by phytoplankton incubation experiments. On the basis of the observation and incubation results, we propose a new isoprene production process—dark production of isoprene by phytoplankton—which is not directly associated with the photosynthetic production of isoprene.

2. Methods

2.1 Shipboard observations and seawater sampling

Funka Bay is separated from the northwestern North Pacific Ocean by an 80-m-deep sill. The bay water exchanges with the open-ocean water of the North Pacific twice a year, mainly in early spring and in autumn (Ohtani and Kido 1980). In most years, a massive phytoplankton bloom consisting mainly of diatoms occurs in the surface layer, covering most of the bay from early March to early April (Odate et al. 1993; Kudo et al. 2007). We conducted observations monthly or bimonthly from December 2015 to November

2016 using the Training Ship *Ushio-maru*, operated by the School of Fisheries Sciences, Hokkaido University. Seawater was sampled at the center of Funka Bay (Station [St.] 30; 42°16.2 N, 140°36.0 E; bottom depth, 96 m; Fig. 1) on 15 December 2015, and 5 February, 22 March, 13 April, 17 May, 29 July, 27 August, and 1 November 2016. Conductivity-temperature-depth (CTD; SBE-19plus, Sea-Bird Electronics, Inc., Washington, USA) observations without water sampling were carried out at 24 stations in the bay on 7 March and other dates.

Our methods for Funka Bay observations and seawater measurements have been recently reported (Shimizu et al. 2017). Seawater samples were collected in 2-L Niskin bottles attached to a rosette multisampler along with a CTD probe (SBE-19plus) and a photosynthetically-active-radiation (PAR) sensor. PAR measurements in December 2015 and February 2016 were not well executed. Surface seawater was collected with a plastic bucket, and bottom water was collected approximately 1 m above the seafloor with a Van-Dorn sampling bottle. The sampling depths were 0, 5, 10, 20, 30, 40, 50, 60, 65, 70, 75, 80, 85 and "bottom-minus-1" m (approximately 95 m). In December 2015 and February 2016, seawater samples were collected from only 6 and 4 depths, respectively, using a Van-Dorn sampling bottle and a bucket. Seawater aliquots (125 mL) were collected into dark glass bottles, each of which was overflowed with approximately 250 mL of seawater.

Microbial activity was arrested by the addition of 50 μL of saturated mercuric chloride ($HgCl_2$) solution. The bottles were crimp-sealed with a headspace of 0.5 mL by using an aluminum cap and a septum lined with butyl rubber. The sample bottles were kept in the dark at 4°C until pretreatment, which was typically carried out within 2 weeks of sampling.

2.2 Isoprene analysis

Dissolved isoprene was collected from seawater samples by the purge-and-trap method.

156 The total volume of seawater (125 mL) in each sample bottle was introduced into a
157 purge vessel by means of a high-purity nitrogen flow at 20 mL min^{-1} for 7 min, and the
158 dissolved gases were then purged by bubbling with nitrogen at a flow rate of 65 mL
159 min^{-1} for 35 min at 60°C. The purged gases were collected in a cold trap containing
160 Tenax TA (GL Science, Tokyo, Japan) adsorbent resin (10 mg) cooled to –90°C. The
161 cold trap was then sealed with 1/16-inch screw nuts (Swagelok, solon, OH, USA) and
162 stored in a freezer (–30°C) prior to analysis by gas chromatography-mass spectrometry
163 (GC-MS), typically within two weeks. The purge efficiencies for isoprene were nearly
164 100%.

165 Concentrated isoprene in the cold trap was thermally desorbed (200°C) from
166 the resin and transferred to an automated preconcentration GC-MS system (Agilent
167 5973, 6890; Agilent Technologies, Santa Clara, CA, USA) equipped with a capillary
168 column (CP-Porabond Q, 0.32 mm × 50 m, Agilent Technologies).

169 Gravimetrically-prepared standard gas (Taiyo Nissan, Inc., Tokyo, Japan)
170 containing isoprene at 10 parts per billion (ppb) was used to calibrate the GC-MS
171 system. The standard gas measurements were carried out once a day. The analytical
172 precision for isoprene of ±4% (=standard deviation/mean) was evaluated from the
173 repetitive measurement (n = 6) of a water-based standard solution. Details of the
174 GC-MS analysis are described elsewhere (Ooki and Yokouchi 2011a, b, Ooki et al.,
175 2015b).

176

177 **2.3 Chl-a and nutrient concentrations**

178 Chl-a concentrations in discrete seawater samples (100 mL) were measured by the
179 Welschmeyer method (Welschmeyer 1994) using a fluorometer (10-AU-005, Turner
180 Designs, San Jose, CA, USA). Concentrations of nitrogenous nutrients (NO_3^-, NO_2^-,
181 and NH_4^+) in discrete seawater samples were measured by the colorimetric method with
182 a QuAAtro 2-HR system (BL-tec, Osaka, Japan; Seal Analytical, Norderstadt,

183 Germany). Analytical precisions were 0.5% for NO_3^-, NO_2^-, and NH_4^+ as determined
184 by repetitive measurement (n = 5) of reference seawater for nutrient standards (KANSO,
185 standard Lot BT, Osaka, Japan). We used the combined concentrations of these
186 compounds as the dissolved inorganic nitrogen (DIN) concentration.
187
188 **2.4 Incubation experiments**
189 Isoprene production was investigated in two phytoplankton incubation experiments.
190 Culture medium seawater was collected from a coastal region near Hokkaido in the
191 northern Japan Sea (salinity = 33.8) and was filtered through an acid-cleaned 0.22 μm
192 cellulose membrane filter (Millipore). The filtered seawater was autoclaved for 20 min
193 at 121°C. Subcultured strain of *Thalassiosira weissflogii* CCMP1336 was added to the
194 culture medium with f/2 nutrient (Price et al.,, 1989). The initial cell density of
195 *Thalassiosira weissflogii* in the medium was controlled to be approximately 1000 cells
196 mL^{-1}. One-hundred milliliters of culture medium was poured into a glass bottle (120
197 mL), which was crimp-sealed with an aluminum cap and septum. These operations were
198 done in a clean bench. Glass bottles were moved to an incubator at temperature of 20°C,
199 and light intensity of 100 μmol photon m^{-2} s^{-1} from an LED light with a light:dark cycle
200 of 13-h:11-h. A culture without diatoms was incubated as a control. Fig 2 (upper panel)
201 is a schematic diagram showing the culture conditions and the process for isoprene
202 collection from the incubation bottles. Incubation lasted 85 days in experiment I and 53
203 days in experiment II. Incubation bottle in experiment II was moved into continuous
204 dark conditions on day 12 to investigate the dark production of isoprene. The number of
205 experiment bottle and control bottle was one for each experiment.
206 Head-space gas in incubation bottles was collected every 2 or 3 days during the
207 incubation periods (53 or 85 d). Pure air (20% O_2 and 80% N_2) mixed with CO_2 (400
208 ppm) was introduced into the bottle through an injection needle at a flow rate of 50 mL
209 min^{-1} for 30 min while the culture medium was stirred by a magnetic stirrer. The

head-space gas was collected through another needle, and the water vapor in the gas was removed by using a Nafion drying tube (Perma Pure, Lakewood, NJ, USA). To concentrate isoprene, the sample gas was then introduced into a cold trap containing 10 mg Tenax TA absorbent resin at –90°C using a Free Piston Stirling Cooler (FPSC; Twinbird, Ltd., Tsubame-Sanjo, Japan). The cold traps were stored in a freezer at –25°C until GC-MS analysis. After the collection of isoprene, the incubation bottle was opened by removing the butyl rubber septum, and 250 μL of culture medium was collected to measure the chl-a concentration and cell density. The bottle was then re-sealed with septum and aluminum cap and the incubation continued. The 250 μL sample was diluted with 5.0 mL of filtered seawater. Cell density in the diluted sample was measured by triplicate cell counts by an optical microscope, and chl-a concentration in the diluted sample was measured by Welschmeyer method after filtration and DMF extraction.

The collection efficiency for isoprene in the incubation bottles using this method was 80% at room temperature (about 20°C). We adjusted the isoprene production rates in the incubation bottles assuming that 20% of the isoprene remained in the bottle after each collection. Calculation method of isoprene production rate was drawn in a lower panel of Fig 2.

The mean concentration of isoprene in a series of control incubation bottles—with culture medium but no diatoms—was 11.7 ± 1.7 pmol L^{-1} (n = 40). This means that there was on average 1.17 ± 0.17 pmol of isoprene contamination in the incubation bottles (water volume of 0.1 L and gas head-space of 0.02 L). Contamination likely occurred when the bottle was opened to collect water for chl-a analysis. Although we did not measure the isoprene concentration in the laboratory air, ambient room-air concentrations were reported as 1.4 ppb in China (Duan et al. 2016) and 3.6–7.2 ppb in the UK (Wang et al. 2017), which are several times higher than in outside air. The main source of isoprene in room air is human breath (Stonner et al. 2017). If the gas head-space in the incubation bottles (0.02 L) was replaced with room air having an

isoprene concentration of 1.4–7.2 ppb, the isoprene contamination would amount to 1.3–6.4 pmol. We assumed the detection limit for the difference in isoprene concentrations between the incubation bottles and the control bottles ([Incubation bottle C_5H_8] – [Control C_5H_8]) to be two times the standard deviation (=2 × 1.7 pmol L^{-1}) of the blank (control) measurement.

Isoprene concentrations in the incubation bottles were 76–607 pmol L^{-1} under light-dark cycle conditions (hereinafter, light conditions) (28 samples in experiment (I) + 4 samples in experiment (II)), and 10.5–38.3 pmol L^{-1} under dark conditions (15 samples in experiment (II)). The concentration differences between incubation and control bottles were 69.3–570 pmol L^{-1} in the light and –2.4 to 138.8 pmol L^{-1} in the dark. The concentration differences for 5 samples (5 sets of incubation and control bottles) under dark conditions were below the detection limit (<3.4 pmol L^{-1}), whereas those for 10 samples under the dark were above the detection limit (13.7 ± 10.1 pmol L^{-1}, mean ± standard deviation, n = 10).

3. Results and discussion

3.1 Hydrographic features

Funka Bay is influenced by two main water masses that enter from the open ocean: Tsugaru (T) water that originates from the subtropical North Pacific Ocean and Oyashio (O) water that originates from the subarctic North Pacific. In addition, there are two water masses formed by changes in the bay: winter (W) water is formed by winter cooling of T water, and summer (S) water is formed by summer warming and salinity lowering of O water. In this study, we classified the water masses in the bay according to the temperature–salinity ranges listed in Table 1, which are modified from Ohtani and Kido (1980) because the temperature range of O water was expanded for this study.

The temperature–salinity ranges for classification of the water masses are plotted in Figure 3. In addition to the four main water masses—T, W, O, and S—we

264 defined transition water types: mixing types ‘WO’, ‘WOT’, and ‘ST’, and temperature
265 changing types ‘TW’ and ‘OS’. These transition waters filled in areas of the
266 temperature–salinity ranges not occupied by the four main water masses (Fig. 3). For
267 example, WO water is a transition water between W and O waters.
268 We produced vertical profiles of temperature and salinity at the sampling
269 station (St. 30) in Funka Bay (Fig. 4). We used the temperature–salinity ranges of the
270 six water masses to show the temporal variation of the water-mass structure at St. 30 in
271 the bay (Fig. 5).
272 In December, Funka Bay was occupied by high-salinity T water at all depths. This
273 water cooled in winter, transitioning to TW water in February and W water in March.
274 Low salinity O water was found at the surface in the mouth of Funka Bay on 7 March
275 (not shown in Fig. 5), and this water flowed to the sampling station (St. 30), changing
276 the water there from W water to WO water on 22 March (0–10 m), to O and WO water
277 (0–35 m) on 13 April, and to O and WO water (0–75 m) on 17 May (Fig. 5). The W
278 water remained in the bottom layer (75–95 m) from March to May. The O water was
279 warmed by solar radiation in summer, changing to S water in July (0–18 m). In July and
280 August, high-salinity T water flowed in the middle to deep layers of the bay from the
281 open ocean, changing the S water to ST or WOT waters (18–95 m) in July, to T water
282 (72–95 m) in August, and to T water throughout the water column (0–95 m) in
283 November.
284
285 **3.2 Seasonal variation in vertical profiles of biochemical parameters and light**
286 We generated separate plots of the vertical distributions of isoprene (C_5H_8), apparent
287 oxygen utilization (AOU), DIN, and chl-a for December–April (Fig. 6a) and May–Nov
288 (Fig. 6b). Vertical profiles of PAR for March, April, May, July, and August are
289 presented separately (Fig. 7). We also determined the depth at which PAR was 0.5% of

surface PAR, and the mixed-layer depth, defined as the depth at which the potential density is higher by 0.05 kg m^{-3} than that at the reference depth of 5 m (Fig. 6a, b).

3.2.1 Chl-a, DIN, and oxygen concentrations

In February, chl-a concentrations were uniform for the depth range of 0–85 m with an mean of 0.84 μg L^{-1}. The chl-a concentrations increased substantialy from February to March at all depths. The mean on 22 March was 9.3 μg L^{-1}, and maxima were found at 5 m (16.8 μg L^{-1}) and 95 m (11.7 μg L^{-1}). These concentrations are consistent with previously reported maximum values (5–20 μg L^{-1}) over a period from February to April during the spring diatom bloom at the same location in Funka Bay (Odate et al. 1993; Kudo et al. 2007). We suggest that we observed the peak of the spring diatom bloom on 22 March. The concentration maximum of chl-a in the deepest water on 22 March (9.3 μg L^{-1}) suggested that large amounts of diatoms were suspended near the bottom during the peak of (or just after the peak) diatom bloom. The data suggest that large amounts of diatom aggregates produced in the surface euphotic zone had been sinking from the surface to the bottom.

Chl-a concentrations decreased from March to April at all depths. Nevertheless, there were still high concentrations of chl-a (3.0–5.7 μg L^{-1}) in April at 30–50 m, which was below the mixed-layer depth of 11 m. The depth of 0.5% of surface PAR, which is thought to be the compensation depth (photosynthesis = respiration), was 15 m in March, and the PAR became zero in the middle layer shallower than 60 m in March and April. Presumably the large amounts of phytoplankton below 60 m in March and April could not photosynthesize in the dark. Negative values for AOU found at depths of 0–40 m in March and 0–30 m in April indicated that there was net production (photosynthesis > respiration) in those layers. The decrease of the DIN concentrations in the surface mixed layer from February (8.1–12.7 μmol L^{-1} at 0–95 m) to March (<0.05–3.1 μmol L^{-1} at 0–35 m) indicated that nutrients in the surface mixed layer of the bay

had been consumed by the massive diatom bloom in March. Despite DIN depletion in the surface mixed layer (<0.05 μmol L^{-1} at 0–11 m) in April, there were moderate chl-a concentrations (0.7–2.7 μg L^{-1}) at the surface. It is possible that the inflow of O water in April supplied nutrients to the surface of the bay and maintained new production in the surface waters.

There was a clear chl-a maximum at the surface (0 m) on 29 July (0.71 μg L^{-1}), despite DIN depletion (<0.05 μmol L^{-1}) in the mixed layer. We suggest that new production at the surface was supported by a temporary supply of nutrients through freshwater inputs (river and rain) before 29 July because the salinity decreased by 0.9 at 5-m depth from 17 May to 29 July. On 27 August, there was a distinct chl-a maximum (approximately 0.31 μg L^{-1}) at 20–50 m depths, just below the surface mixed layer (17 m), and within the euphotic zone with sufficient DIN (0.52–8.2 μmol L^{-1}) to support primary production. This type of chlorophyll maximum is commonly observed in summer in the open ocean and is referred to as a "subsurface chlorophyll maximum". The subsurface chl-a maximum layer shallower than 30 m was oligotrophic condition with low nutrient level (DIN = 0.52 – 0.70 μmol L^{-1}). In November, there were moderate chl-a concentrations (0.87–1.04 μg L^{-1}) in the surface mixed layer (0–57 m) with high concentrations of DIN (3.50–3.80 μmol L^{-1}).

3.2.2 Isoprene (C_5H_8)

In December and February, isoprene concentrations were vertically uniform from winter deep mixing, averaging 21.8 and 22.8 pmol L^{-1}, respectively. These mean values were half of the annual mean of 42.8 pmol L^{-1} during the observation period and consistent with the open-ocean mean of 19.7 pmol L^{-1} in the northwest Pacific near Japan in April (Kurihara et al. 2010).

The concentrations increased from 5 February to 22 March over the depth range of 0–50 m. We suggest that there was photosynthetic production of isoprene

during the massive diatom bloom in March. High isoprene concentrations in the mixed layer (0–35 m) on 22 March were vertically uniform within the narrow range of 56.8–67.8 pmol L^{-1}. The concentrations in this depth range decreased slightly from 22 March to 13 April. Note that the isoprene concentrations in the bottom layer (80–95 m) increased substantially from 22 March (mean, 20.7 pmol L^{-1}) to 13 April (28.1 pmol L^{-1}), where W water persisted during this period. We present calculated isoprene production rates in the surface mixed layer (0–35 m) in March and the bottom layer (80–95 m) from March to April in section 3.3.

From May to August, there was a substantial isoprene concentration maximum in the subsurface O or ST water at depths of 20–40 m, just below the surface mixed layer (subsurface layer). The isoprene concentrations in this subsurface water, which was shallower than the depth of 0.5% surface PAR, substantially increased from 17 May (mean, 42.4 pmol L^{-1}) to 29 July (86.4 pmol L^{-1}) and 27 August (124.9 pmol L^{-1}). We suggest that these increases are due to photosynthetic production of isoprene and the fact that isoprene produced below the surface mixed layer was prevented from sea–air out-gassing.

3.3 Isoprene production rates

We estimated in-situ production rate of isoprene in seawater of Funka bay from an increment of isoprene during a period between two observation dates. The in-situ production means net-production including biogenic production of isoprene mainly by phytoplankton, bacterial degradation, and chemical degradation. We supposed that the biological production is about ten times of the total degradations based on results of global isoprene flux model by Palmer and Shaw (2005). To minimize the effect of horizontal transport of isoprene, we selected periods and depths where the water masses had been stayed within the bay as shown in Fig 5. However, the effect of horizontal transportation of isoprene in the same water mass within the bay cann't be still ruled out.

We additionally conducted a shipboard observation in Funka bay at the station of 30 (center of the basin) and 23 (back of the basin, 14 km away from station 30) in May of 2018. The difference of isoprene concentrations between the two stations in the depth range of 20 – 30 m, which was below the mixed layer within the euphotic layer, was 11%. We notice that the following estimations of isoprene production rate have uncertainty of 11% or more owing to possible horizontal transportation effect.

3.3.1 In-situ isoprene production rates in the surface mixed layer during the spring diatom bloom

Isoprene concentrations increased by 42.4 pmol L^{-1} in the surface mixed layer (0–35 m) between 5 February and 22 March during a massive diatom bloom. In January - March 2016, diatom aggregates were collected by a NORPAC net with a 100-μm mesh by the Training Ship *Ushio-maru*, which was collecting zooplankton at the same station in Funka Bay (no chl-a data were collected). The volume of aggregates in the NORPAC samples started to increase since 25 February. Eight days mean of surface chlorophyll-a concentration in 5 – 12 March was much higher than that in 26 February to 4 March. (MODIS aqua, Sea-viewing Wide Field-of-view Sensor (SeaWiFS) Ocean Color Data, NASA OB.DAAC, Greenbelt, MD, USA. http://doi.org/10.5067/ORBVIEW-2/SEAWIFS_OC.2014.0.) We assumed that the spring diatom bloom had started around 25 February and that the massive diatom bloom that we observed in Funka Bay on 22 March had persisted for the previous 26 days (=T_{bloom}). The isoprene production rate ($P_{Mar(0–35\ m)}$) was estimated by the following equation.

$$P_{Mar(0–35\ m)} = (\Delta C_5H_8 + F_{sea–air})/[\text{chl-a}]_{(0\text{-}35\ m)}/T_{bloom}\ , \quad (1)$$

where ΔC_5H_8 is the increase in the amount of isoprene (=1.5015×10^6 pmol m^{-2}) in the surface mixed layer (0–35 m) between the observation dates on 5 February and 22 March (gray-shaded areas in Fig. 8), and [chl-a]$_{(0\text{-}35m)}$ is the time-integrated average of chl-a (=1.4×10^5 μg m^{-2}) amount from 25 February to 22 March in the same layer. We used chl-a fluorescence surface monitoring data (Thermosalinograph XR-420CTX; Richard Brancker Research Ltd. Ottawa, ON Canada; minimum detectable level: 0.02 μg L^{-1}) measured at the same station on 5 and 25 February and 8 and 22 March (Yamaoka et al., *submitted*) to interpolate the surface chl-a concentration from 25 February to 22 March. The calculation method is shown in Fig. 9. We obtained exponential curve ($y = 0.521\ e^{0.0567x}$) of chl-a increase in the surface during the period. The time-integrated average of chl-a amount in the depth range of 0 – 35 m from 25 February to 22 March was calculated using the same exponential increase rate. $F_{sea–air}$ is the time-integrated sea-to-air flux of isoprene during the diatom bloom from 25 February to 22 March. The fluxes were calculated according to Ooki et al. (2015) using hourly wind speeds at the Muroran meteorological weather station on the coast of Funka Bay (Fig. 1), and a Henry's law constant of isoprene in seawater (Ooki and Yokouchi, 2011b). Mean isoprene concentration (45.0 pmol L^{-1}) in the surface water on 5 February and 22 March was used for the flux calculation. Atmospheric isoprene concentration was assumed to be 80 patm, which is half of the mean value observed over a forest in Hokkaido (Ieda et al. 2006), based on an atmospheric lifetime of 1–2 h and a transport time of about 1–2 h from the surrounding forest to the center of Funka Bay. The sea-to-air flux was estimated to be 5.36×10^4 pmol m^{-2} d^{-1}. The time-integrated flux, $F_{sea–air}$, was 1.45×10^6 pmol m^{-2}. The settings of production rate calculation were summarized in Table 2. The $P_{Mar(0–35m)}$ was estimated to be 0.82 pmol (μg chl-a)$^{-1}$ d^{-1}. Note that estimated production means net production of isoprene including both productions and consumptions in seawater, and we assumed that the seawater in the surface layer (0 – 35 m) was not vertically mixed with lower layer.

3.3.2 In-situ production rate of isoprene in the subsurface layer in July–August

The isoprene concentrations in ST water at 20–40 m showed a substantial increase of 38.5 pmol L^{-1} (=ΔC_{C5H8}) from 29 July (mean, 86.4 pmol L^{-1}) to 27 August (124.9 pmol L^{-1}). This depth range was just below the surface mixed layer (17 m in July and 18 m in August) and shallower than the depths of 0.5% of surface PAR (45 m in July and 51 m in August). A distinct chl-a maximum was found within that depth range in August (mean, 0.29 μg L^{-1} = $[\text{chl-a}]_{(20\text{-}40\text{m Aug})}$). We suggest that the isoprene increase from July to August was due to photosynthetic production of isoprene in the euphotic zone. Note that effects of high salinity T water inflows were obvious in July in that depth range compared with the lower salinity profile in May, and the salinity profile was found to become vertically smooth in August (Fig. 4). We assumed that the water in that depth range (20 – 40 m) had been stayed in the bay since 29 July until 27 August, on ground that the basin-wide anticyclonic circulation formed in the surface of the bay in summer (Miyake et al., 1998), which would restrict the water exchange between the basin of the bay and open ocean, was found to be strengthened in July - August 2016 analyzed by Acoustic Doppler Current Profiler (ADCP) observation data at the same station (Onishi et al., 2017).

The isoprene production rate per unit chl-a (=$P_{Aug(20–40m)}$) was calculated by the following equation using the mean $[\text{chl-a}]_{(20\text{-}40\text{m July-Aug})}$ (0.18 μg L^{-1}) and the time interval of 29 d between the observation dates in July and August. Note that the sea-to-air flux can be omitted for the calculation below the surface mixed layer, and we assumed that the seawater in the subsurface layer (20 – 40 m) was not vertically mixed with upper and lower layers.

$$P_{Aug(20–40m)} = \Delta C_{C5H8}/[\text{chl-a}]_{(20\text{-}40\text{m})}/29\ \text{d} \quad (2)$$

$P_{Aug(20–40m)}$ was calculated as 7.38 pmol (μg chl-a)$^{-1}$ d^{-1}, which is much higher than the rate during the spring diatom bloom in March (0.82 pmol [μg chl-a]$^{-1}$ d^{-1}).

3.3.3 Comparison between isoprene production in-situ and in diatom incubation experiments under light conditions

We followed cell densities, isoprene production, and chl-a concentrations in both experiments I and II (Figs. 10 and 11, respectively). Chl-a concentrations in the incubation bottles increased exponentially from 3.4 to 301 μg L^{-1} in the first 13 days of experiment I, and from 4.5 to 165 μg L^{-1} in the first 8 days of experiment II. These intervals are considered the exponential growth phase. The chl-a concentrations gradually increased to around 307 μg L^{-1} over the next 7 days of experiment I, and to 187 μg L^{-1} over the next 6 days of experiment II. These intervals are referred to as the "steady phase". The incubation bottles in experiment II were moved into continuous dark conditions after the steady phase. The chl-a concentrations in experiment I decreased from 307 μg L^{-1} on day 20 to 66 μg L^{-1} on day 48. This interval is called the "decline phase". After the decline phase, the concentrations varied within a narrow range (53–59 μg L^{-1}) for 24 days. This interval is called the "stagnation phase".

We calculated the chl-a content per cell (Figs. 10 and 11, middle panels). The chl-a content was 2–4.6 (mean, 3.1) pg chl-a cell^{-1} in the exponential growth and steady phases of experiment I, and was the highest (1.9–6.0; mean, 4.7 pg chl-a cell^{-1}) in the stagnation phase.

The production rates per unit chl-a in the exponential growth phase were 0.55–1.6 (mean, 1.1) pmol (μg chl-a)$^{-1}$ d^{-1} for experiment I and 1.8–2.4 (mean, 2.2) pmol (μg chl-a)$^{-1}$ d^{-1} for experiment II. The isoprene production rates normalized to chl-a concentration and cell density were the highest in the exponential growth phase and the lowest in the steady and decline phases (mean, 0.35 pmol [μg chl-a]$^{-1}$ d^{-1}) in experiment I. Our incubation results are consistent with previous diatom incubation results of 0.65–

1.26 pmol (μg chl-a)$^{-1}$ d^{-1} (*Chaetoceros debilis, C. neogracilis*) under PAR of about 100 μmol photon m^{-2} s^{-1} (Bonsang et al. 2010), which is the same PAR level as in our experiment, and 2.66 pmol (μg chl-a)$^{-1}$ d^{-1} (*Thalassiosira weissflogii*) with a high PAR of 300 μmol photon m^{-2} s^{-1} (Exton et al. 2013).

The in-situ isoprene production rate during the spring diatom bloom ($P_{\mathrm{Mar(0–35m)}}$; 0.82 pmol [μg chl-a]$^{-1}$ d^{-1}) is consistent with our diatom incubation results in steady and decline phases (means; 0.35 – 2.2 pmol [μg chl-a]$^{-1}$ d^{-1}). In contrast, the in-situ production rate in summer (July–August) ($P_{\mathrm{Aug(20–40m)}}$; 7.38 pmol [μg chl-a]$^{-1}$ d^{-1}) was much higher than the diatom incubation results and in-situ $P_{\mathrm{Mar(0–35m)}}$. The difference between $P_{\mathrm{Mar(0–35m)}}$ and $P_{\mathrm{Aug(20–40m)}}$ was likely due to the difference in dominant phytoplankton species in each season. The main phytoplankton in Funka Bay during the spring bloom are large diatoms (cell size > 10 μm) (Odate 1989). In the early phase of the diatom bloom in February–March, *Thalassiosira spp.* are the most abundant diatoms, and toward the end of the bloom, *Chaetoceros spp.* become the dominant diatoms (Shinada et al. 1999). During the summer, cell density of phycoerythrm-rich cyanobacteria, such as *Synechococcus sp.*, rapidly increased from spring (10^5 cells/L) to summer (10^8 cells/L) in the upper stratified low nutrient layer, predominating the cell density of pico-phytoplankton less than 2 μm (Odate 1989). Synechococcus occupied approximately 10 % of depth-integrated Chl-a concentration within euphotic zone (0 – 39 m; 1 % of surface PAR) in Funka bay in August 2010 (Isada et al., 2017), while it occupied approximately 30 % of Chl-a in the oligotrophic surface water (Isada et al., 2015). The subsurface layer (20 – 40 m) in August 2010 at the same station was rich in nutrients (NO_2^- + NO_3^- = 0.9 – 3.4 μmol L^{-1}) and low temperature (5 – 10 °C) (Hioki et al., 2015), while that in July and August 2016 was oligotrophic (NO_2^- + NO_3^- = 0.02 – 0.28 μmol L^{-1} and NO_2^- + NO_3^- = 0.02 – 1.42 μmol L^{-1}, respectively) and high temperature (12 – 20 °C) (this study). Since picoplankton, such as Synechococcus prevails in high temperature oligotrophic water in the

505 Mediterranean Sea (NO_2^- + NO_3^- < 1 μmol L^{-1}) (Agawin et al., 2000), we supposed that
506 phycoerythrm-rich cyanobacteria, such as Synechococcus sp., prevailed in the
507 subsurface layer of Funka bay in July – August 2016.

508 The diatom used in our incubations, *Thalassiosira weissflogii*, had isoprene
509 production rates of 0.27–2.4 pmol (μg chl-a)$^{-1}$ d^{-1} (this study). Bonsang et al. (2010)
510 reported that the cyanobacterium *Synechococcus sp.* had an isoprene production rate of
511 4.97 pmol (μg chl-a)$^{-1}$ d^{-1}, the highest among the nine species they tested. This
512 production rate is consistent with our results for in-situ $P_{Aug(20–40m)}$. Furthermore, the
513 isoprene production rates for diatom (Meskhidze et al., 2015; Exton et al., 2013) and
514 cyanobacteria (Shaw et al., 2003; Exton et al., 2013) rose with temperature increase.

515 We concluded that the relatively low value for in-situ $P_{Mar(0–35m)}$ during the
516 spring bloom and the high value for $P_{Aug(20–40m)}$ in summer were attributable to isoprene
517 production by large diatoms such as *Thalassiosira* spp. and phycoerythrin containing
518 organisms such as *Synechococcus* spp., respectively. The high value for $P_{Aug(20–40m)}$
519 would be also attributable to higher isoprene productions by diatom and cyanobacteria
520 at higher temperature.

521

522 **3.3.4 Isoprene production in the dark bottom layer of Funka Bay**

523 The isoprene concentration in the bottom layer (80–95 m) of the bay increased by 7.4
524 pmol L^{-1} (=ΔC_{C5H8}) from 22 March to 13 April in the W water, where there were no
525 temperature or salinity changes. There was a high concentration of chl-a (9.86 μg L^{-1}) in
526 the bottom layer ($[chl\text{-}a]_{bottom}$) on 22 March, whereas it was low (0.22–0.65 μg L^{-1}) on
527 13 April. The large numbers of diatoms produced in the spring bloom in March were
528 likely sinking from the surface euphotic zone to the bottom layer during this period,
529 blocking the sunlight from the bottom layer. On the basis of these observations, we
530 hypothesize that isoprene is produced by phytoplankton in the dark. The in-situ

production rate of isoprene in the dark bottom layer, $P_{Mar(80–95m)}$, was calculated using the following equation.

$$P_{Mar(80–95m)} = \Delta C_{C5H8}/[\text{chl-a}]_{bottom}/T_{dark}\ , \qquad (3)$$

where T_{dark} (days) is the time-period for isoprene production in the dark by diatom cells suspended in the bottom layer between 22 March and 13 April. We assumed T_{dark} to be 6–22 days. This means that the high concentrations of chl-a in the bottom layer could have persisted for more than 6 days after 22 March. The minimum time of 6 days was roughly calculated from the sinking time of diatom aggregates from the surface to the bottom layer (95 m) at a sinking velocity of 14.4 m d^{-1} (=1 cm min^{-1}). The sinking velocity was roughly measured in a simple experiment where we observed diatom aggregates collected in a bottle. Seebah et al. (2014) have reported the sinking velocity of *Thalassiosira weissflogii* aggregates of a size that could be trapped by the mesh in our NORPAC net (>0.5 mm) ranging between 8 and 110 m d^{-1}. The in-situ $P_{Mar(80–95m)}$ in the dark was estimated at 0.03–0.13 pmol (μg chl-a)$^{-1}$ d^{-1}, which is 4–16% of in-situ $P_{Mar(0–35m)}$ in the light.

We tested for the dark production of isoprene in incubation experiment II (Fig. 11). On day 12 of the incubation, during the steady phase, the incubation bottle was moved into continuous dark conditions. In the dark, chl-a concentrations decreased sharply from 187 μg L^{-1} on day 14 to 9.9 μg L^{-1} on day 35, and they remained low (8.3–11.7 μg L^{-1}) for 14 days until the end of the incubation (day 53). The mean production rates were 0.19 pmol (μg chl-a)$^{-1}$ d^{-1} (=P_{dark}) or 2.9 × 10^{-7} pmol $cell^{-1}$ d^{-1}, which are 9% and 6%, respectively, of those in the exponential growth phase in the light. This production rate during the incubation was somewhat higher than the in-situ $P_{Mar(80–95m)}$ in the dark (0.03–0.13 pmol [μg chl-a]$^{-1}$ d^{-1}).

Many of previous incubation studies (e.g. Bonsang et al., 2010, Exton et al., 2013, Dani et al., 2017) have not noticed isoprene production in the dark; however, the results of some of these studies seem to show that small amounts of isoprene were emitted in the dark. In a plot of isoprene production rate vs. PAR intensity (Fig. 2 in Bonsang et al. 2010), it looks like the phytoplankton produced isoprene at 0–0.2 pmol (μg chl-a)$^{-1}$ d^{-1} in the dark (PAR = 0), which is about 0–15% of their production rate under light conditions. Incubation results from another study show that the isoprene production rate per cell by the cyanobacterium *Prochlorococcus* sp. dropped sharply in the dark, and the rate after 48 h in the dark was reported to be 16% of the rate in exponential growth phase in the light (Fig. 4c in Shaw et al. 2003). A recent incubation study reported values of isoprene production rate in the dark by diatom, *Thalassiosira weissflogii*, to be 0.48 pmol (μg chl-a)$^{-1}$ h^{-1} at 18 °C, which was 14 % of that under the light with irradiance intensity of 150 μmol m^{-2} s^{-1} (Meskhidze et al., 2015).s As for isoprene production by macroalgae, the green macroalgae *Ulva intestinalis* produced isoprene in the dark at 0.6 pmol (g dry-wt)$^{-1}$ h^{-1}, which was 16% of that in the light (Broadgate et al. 2004). Apparently isoprene can also be formed by higher plants via the breakdown of stored carbohydrates when photosynthesis is blocked (Lerdau et al. 1997). Broadgate et al. (2004) have inferred a similar pathway for isoprene production by marine macroalgae in the dark.

We conclude that isoprene production rate by diatom in the dark raged from 4% to 16% of that in the light associated with their photosynthesis. The contribution from dark production would be important in a dim subsurface layer below the compensation depth (around 0.5% of surface PAR) where the chl-a concentration maximum is found, and at night. Note that our values for in-situ $P_{\mathrm{Mar(0–35m)}}$ and $P_{\mathrm{Aug(20–40m)}}$ include nighttime production (P_{dark}).

3.3.5 Isoprene emission factor (EF)

584 In a recent study, the isoprene production rate per unit chlorophyll (P_{chl}; pmol [μg
585 chl-a]$^{-1}$ h^{-1}) was calculated as a function of PAR (I; μmol photon m^{-2} s^{-1}) using the
586 following equation (Gantt et al. 2009; Booge et al. 2018):
587
588 $$P_{chl} = EF \times (\ln I)^2 , \quad (4)$$
589
590 where EF is the emission factor of isoprene measured by incubation experiment for
591 specific phytoplankton species. This equation has been used for the global isoprene
592 production estimate (Gantt et al. 2009) and basin-scale isoprene budgets (Booge et al.
593 2018).
594 In this study, the in-situ isoprene EF in Funka Bay was calculated from our
595 results for production rates ($P_{Mar(0–35m)}$ and $P_{Aug(20–40m)}$) and observed PAR. The values
596 for $P_{Mar(0–35m)}$ and $P_{Aug(20–40m)}$ were converted to 0.0680 pmol (μg chl-a)$^{-1}$ h^{-1} and 0.527
597 pmol (μg chl-a)$^{-1}$ h^{-1}, respectively, by dividing by the daytime hours (12 hours in March
598 and 14 hours in August). The surface PAR at noon in March was 1200 μmol photon m^{-2}
599 s^{-1}, and that in August was 2000 μmol photon m^{-2} s^{-1}. The amount of solar radiation
600 (300–2000 nm) on a clear day in March at the Muroran weather station was 2.7 MJ m^{-2}
601 and that in August was 3.2 MJ m^{-2}. We converted the solar radiation measured at the
602 weather station to the surface PAR at St. 30 by multiplying by a factor of 440
603 (=1200/2.7) in March and 620 (=2000/3.2) in August. The depth profile of PAR was
604 determined using the measured PAR attenuation profiles (Fig. 7).
605 The mean values of I and (Ln I)^2 from 0 to 35 m depth in daytime (0700–1900
606 local time) from 25 February to 22 March were 46.2 μmol photon m^{-2} s^{-1} and 6.0,
607 respectively, and those from 20 to 40 m depth in daytime (0600–2000 local time) from
608 29 July to 27 August were 26.9 μmol photon m^{-2} s^{-1} and 8.3. The in-situ $EF_{Mar(0–35m)}$
609 and $EF_{Aug(20–40m)}$ were calculated as 0.011 and 0.063, respectively. The in-situ $EF_{Mar(0–}$

610 $_{35m)}$ during a massive diatom bloom was somewhat higher than the EF for diatoms
611 (0.0064) reported by Booge et al. (2018).

612 The in-situ $EF_{Aug(20–40m)}$ of 0.063 was higher than the EFs (0.0053–0.0176) of
613 seven phytoplankton species as summarized by Booge et al. (2018). The high in-situ
614 $EF_{Aug(20–40m)}$ in the subsurface layer was likely due to the photosynthetic characteristics
615 of the prevailing planktons having pigments other than chl-a (e.g. phycoerythrin), such
616 as Synechococcus spp.,, in summer in Funka Bay, and to higher emission rate at higher
617 temperature. Barlow and Alberte (1985) reported that Synechococcus spp., having the
618 photosynthetic pigment phycoerythrin, photosynthesize maximally at the very low
619 photon flux densities (10–50 μmol photon m^{-2} s^{-1}) found below the surface mixed layer.
620 In contrast, diatoms generally show optimum photosynthesis at high photon flux
621 densities. The estimated high in-situ $EF_{Aug(20–40m)}$ under relatively low light conditions
622 (mean, 26.9 μmol photon m^{-2} s^{-1}) are likely due to low light-adapted phycoerythrin
623 containing planktons, such as *Synechococcus*, with high efficiency photosynthesis and
624 isoprene emission below the surface mixed layer of Funka Bay.
625

626 **4. Conclusions**

627 From the shipboard observations in Funka Bay, Hokkaido, Japan, vertical
628 profiles of isoprene, chl-a, dissolved oxygen, nutrients, and physical parameters
629 (temperature, salinity, and PAR) from the surface to the bottom layer (1 m above the sea
630 floor at 96 m depth) were obtained monthly or bimonthly from December 2015 to
631 November 2016.

632 On 22 March, high concentrations of chl-a (mean; 9.3 μg L^{-1}) were found in the
633 total depths with two distinct maxima of 16.8 μg L^{-1} at the surface (5 m) and 11.7 μg L^{-1}
634 at the bottom water (95 m), indicating the massive diatom spring bloom and subsequent
635 settling of diatom cells from the surface to the bottom. We found increases in
636 concentrations of isoprene in the surface mixed layer (0 – 35 m) from 5 February to 22

March, and the bottom layer (80 – 95 m) from 22 March to 13 April, during the diatom bloom. We calculated the isoprene production rates per unit chlorophyll amount to be 0.82 pmol (μg chl-a)$^{-1}$ d^{-1} in the surface mixed layer and 0.03 – 0.13 pmol pmol (μg chl-a)$^{-1}$ d^{-1} in the bottom layer. On 27 August, concentration maximum of chl-a was found between the mixed layer depth (18 m) and the compensation depth (51 m) with a mean concentration of 0.29 μg L^{-1}. We found the concentration increase of isoprene from 29 July to 27 August in the depth range of 20 – 40 m, forming a distinct maximum of isoprene on 27 August. We calculated the isoprene production rate per unit chlorophyll amount in this depth range to be 7.38 pmol (μg chl-a)$^{-1}$ d^{-1} from July to August.

We could evaluate in-situ productions of isoprene associated with photosynthesis in the surface mixed layer during the early stage of massive spring diatom bloom (February - March) and below the surface mixed layer (subsurface layer) in summer (August), and dark production in the bottom layer during the last stage of the bloom (March – April).

We considered that the difference in photosynthetic production rates in spring (bloom) and summer (post-bloom) is attributed to the respective dominant phytoplankton in the bay: large diatoms in spring such as *Thalassiosira* spp. and *Chaetoceros* spp., and most likely the small cyanobacterium *Synechococcus* spp. in summer. The in-situ isoprene production rate per unit chl-a in the subsurface layer in summer was more than ten times that in the surface mixed layer in the spring diatom bloom. We attributed the calculated high emission factor (EF) as a function of PAR in summer to low light-adapted *Synechococcus* spp., which can efficiently photosynthesize in the dim subsurface layer. High temperature would also contributed to the high isoprene emission in summer. The estimated in-situ isoprene production rates and in-situ EFs were largely consistent with our incubation results and previous incubation studies. It must be noted, however, that the isoprene production properties in the

664 subsurface layer, where there are high isoprene emitters adapted to low light conditions,
665 are different from the results of previous incubations carried out under intense light
666 conditions.

667 We considered that the isoprene production in the bottom layer during the last
668 stage of diatom bloom (March – April) is attributed to the dark production by diatoms
669 settled from the surface to the bottom. We confirmed the dark production of isoprene
670 through diatom incubation experiments, and we found that the isoprene production rate
671 per unit chl-a in the dark ranged from 4% up to 16% of photosynthetic isoprene
672 production rate in the light. This is the first study to clearly document isoprene
673 production by phytoplankton in the dark.

674

675 **Acknowledgments**

676 We thank two anonymous reviewers for their essential comments to improve the
677 calculations of isoprene production rates and the following discussions. We also thank
678 the captain and crew of T/S *Ushio-maru* of Hokkaido University, School of Fisheries
679 Sciences for their help in sampling, and Prof. Kuma for his help in our culture
680 experiments. This study was supported partly by a grant for FYs 2015–2016 Research
681 Projects from the Hokusui Society Foundation, Sapporo, and by grants-in-aid for
682 scientific research from the Japan Society for the Promotion of Science (nos. 24681001,
683 16H02929).

684

685 References

686 Agawin NSR, Daurte CM, Agusti S (2000) Nutrient and temperature control of the
687 contribution of picoplankton to phytoplankton biomass and production. Limol.
688 Oceanogr. 45(3):591-600. doi:10.4319/lo.2000.45.3.0591

689 Alvarez LA, Exton DA, Timmis KN, Suggett DJ, McGenity TJ (2009) Characterization
690 of marine isoprene-degrading communities. Environ. Microbiol., 12, 3280-3291,

691 Doi: 10.1111/j.1462-2920.2009.02069.x
692 Arnold SR, Spracklen DV, Williams J, Yassaa N, Sciare J, Bonsang B, Gros V, Peeken I,
693 Lewis AC, Alvain S, Moulin C (2009) Evaluation of the global oceanic isoprene
694 source and its impacts on marine organic carbon aerosol. Atmos Chem Phys 9:1253–
695 1262. doi:10.5194/acp-9-1253-2009
696 Barlow RG, Alberte RS (1985) Photosynthetic characteristics of
697 phycoerythrin-containing marine *Synechococcus* spp. Mar Biol 86(1):63–74.
698 doi:10.1007/BF00392580
699 Bonsang B, Gros V, Peeken I, Yassaa N, Bluhm K, Zoellner E, Sarda-Esteve R,
700 Williams J (2010) Isoprene emission from phytoplankton monocultures: the
701 relationship with chlorophyll-*a*, cell volume and carbon content. Environ Chem
702 7(6):554–563. doi:10.1071/EN09156
703 Booge D, Schlundt C, Bracher A, Endres S, Zancker B, Marandino CA (2018) Marine
704 isoprene production and consumption in the mixed layer of the surface ocean - a
705 field study over two oceanic regions. Biogeosciences 15(2):649–667.
706 doi:10.5194/bg-15-649-2018
707 Broadgate, WJ, Liss PS, Penkett SA (1997) Seasonal emissions of isoprene and other
708 reactive hydrocarbon gases from the ocean. Geophys. Res. Lett. 44(21):2675–2678.
709 doi:10.1029/97GL02736
710 Broadgate WJ, Malin G, Kupper FC, Thompson A, Liss PS (2004) Isoprene and other
711 non-methane hydrocarbons from seaweeds: a source of reactive hydrocarbons to the
712 atmosphere. Mar Chem (88):61–73. doi: 10.1016/j.marchem.2004.03.002
713 Cleveland CC, Yavitt JB (1998) Microbial consumption of atmospheric isoprene in a
714 temperate forest soil. Appl. Environ. Microbiol., 64(1), 172-177
715 Dani KGS, Benavides AMS, Michelozzi M, Peluso G, Torzillo G, Loreto F (2017)
716 Relationship between isoprene emission and photosynthesis in diatoms, and its

717 implications for global marine isoprene estimates. Mar Chem 189:17–24.
718 doi:10.1016/j.marchem.2016.12.005
719 Duan H, Liu X, Yan M, Wu Y, Liu Z (2016) Characteristics of carbonyls and volatile
720 organic compounds (VOCs) in residences in Beijing, China. Front Environ Sci Eng
721 10(1):73–84. doi:10.1007/s11783-014-0743-0
722 Exton DA, Suggett DJ, McGenity TJ, Steinke M (2013) Chlorophyll-normalized
723 isoprene production in laboratory cultures of marine microalgae and implications for
724 global models. Limnol Oceanogr 58(4):1301–1311. doi:10.4319/lo.2013.58.4.1301
725 Gantt B, Meskhidze N, Kamykowski D (2009) A new physically-based quantification of
726 marine isoprene and primary organic aerosol emissions. Atmos Chem Phys
727 9(14):4915–4927. doi:10.5194/acp-9-4915-2009
728 Guenther AB, Jiang X, Heald CL, Sakulyanontvittaya T, Duhl T, Emmons LK, Wang X
729 (2012) The Model of Emissions of Gases and Aerosols from Nature version 2.1
730 (MEGAN2.1): an extended and updated framework for modeling biogenic emissions.
731 Geosci Model Dev 5(6):1471–1492. doi:10.5194/gmd-5-1471-2012
732 Hackenberg SC, Andrews SJ, Airs R, Arnold SR, Bouman HA, Brewin RJW, Chance RJ,
733 Cummings D, Dall'Olmo G, Lewis AC, Minaeian JK, Reifel KM, Small, A, Tarran
734 GA, Tilstone GH, Carpenter LJ (2017) Potential controls of isoprene in the surface
735 ocean. Glob Biogeochem Cycl 31(4):644–662. doi:10.1002/2016GB005531
736 Ieda T, Kitamori Y, Mochida M, Hirata R, Hirano T, Inukai K, Fujinuma Y, Kawamura
737 K (2006) Diurnal variations and vertical gradients of biogenic volatile and
738 semi-volatile organic compounds at the Tomakomai larch forest station in Japan.
739 Tellus B 5(3):177–186. doi:10.1111/j.1600-0889.2006.00179.x
740 Hioki N, Kuma K, Morita Y, Miura D, Ooki A, Tanaka S, Onishi H, Takatsu T,
741 Kobayashi N, Kamei Y (2015) Regeneration dynamics of iron and nutrients from
742 bay sediment into bottom water of Funka Bay, Japan. J. Oceanogr 71:703-714.
743 doi:10.1007/s10872-015-0312-6

744 Isada T, Hirawake T, Kobayashi T, Nosaka Y, Natsuike M, Imai I, Suzuki K, Saitoh S, -I
745 (2015) Hyperspectral optical discrimination of phytoplankton community structure
746 in Funka Bay and its implications for ocean color remote sensing of diatoms.
747 Remote Sensing of Environment 159:134-151. doi: 10.1016/j.rse.2014.12.006
748 Isada T, Hirawake Nakada S, T, Kobayashi T, Sasaki K, Tanaka Y, Watanabe S, Suzuki
749 K, Saitoh S, -I (2017) Influence of hydrography on the spatiotemporal variability of
750 phytoplankton assemblages and primary productivity in Funka Bay and the Tsugaru
751 Strait. Estur. Coast. Shelf Sci. 188:199-211. doi:10.1016/j.ecss.2017.02.019
752 Lelieveld J, Butler TM, Crowley JN, Dillon TJ, Fischer H, Ganzeveld L, Harder H,
753 Lawrence MG, Martinez M, Taraborrelli D, Williams J (2008) Atmospheric
754 oxidation capacity sustained by a tropical forest. Nature 452:737–740.
755 doi:10.1038/nature06870
756 Lerdau M, Guenther A, Monson R (1997) Plant production and emission of volatile
757 organic compounds. Bioscience 47(6):373–383. doi:10.2307/1313152
758 Kudo I., Yoshimura T., Lee CW, Yanada M, Maita Y (2007) Nutrient regeneration at
759 bottom after a massive spring bloom in a subarctic coastal environment, Funka Bay,
760 Japan. J Oceanogr 63:791–801. doi: 10.1007/s10872-007-0067-9
761 Kurihara MK, Kimura M, Iwamoto Y, Narita Y, Ooki A, Eum Y-J, Tsuda A, Suzuki K,
762 Tani Y, Yokouchi Y, Uematsu M, Hashimoto S (2010) Distributions of short-lived
763 iodocarbons and biogenic trace gases in the open ocean and atmosphere in the
764 western North Pacific. Mar Chem, 118(3–4):156–170. doi:
765 10.1016/j.marchem.2009.12.001
766 Kurihara M, Iseda M, Ioriya T, Horimoto N, Kanda J, Ishimaru T, Yamaguchi Y,
767 Hashimoto S (2012) Brominated methane compounds and isoprene in surface
768 seawater of Sagami Bay: Concentrations, fluxes, and relationships with
769 phytoplankton assemblages. Mar Chem 134:71–79.
770 doi:10.1016/j.marchem.2012.04.001

771 Li JL, Zhai X, Zhang HH, Yang GP (2018) Temporal variations in the distribution and
772 sea-to-air flux of marine isoprene in the East China Sea. Atmos Environ 187:131–
773 143. doi:10.1016/j.atmosenv.2018.05.054
774 Milne PJ, Riemer DD, Zika RG, Brand LE (1995) Measurement of vertical distribution
775 of isoprene in surface seawater, its chemical fate, and its emission from several
776 phytoplankton monocultures. Mar Chem 48:237–244.
777 doi:10.1016/0304-4203(94)00059-M
778 Miyake H, Shibata K, Higaki N (1998) Basin-side circulation flows in Funka Bay,
779 Hokkaido. Umi to Sora, 74(3), 113-123 (in Japanese with English abstract)
780 Moore RM, Wang L (2006) The influence of iron fertilization on the fluxes of methyl
781 halides and isoprene from ocean to atmosphere in the SERIES experiment. Deep Sea
782 Res II 53(20–22):2398–2409. doi:10.1016/j.dsr2.2006.05.025
783 Odate T (1989) Seasonal changes in cell density of cyanobacteria and other
784 picophytoplankton populations in Funka bay, Japan. Bull Plankton Soc Japan
785 36(1):53–61
786 Odate T, Yanada M, Mizuta H, Maita Y (1993) Phytoplankton carbon biomass estimated
787 from the size-fractionated chlorophyll a concentration and cell density in the
788 northern coastal waters from spring bloom to summer. Bull Plankton Soc Japan
789 39(2):127–144
790 Ohtani K, Kido K (1980) Oceanographic structure in Funka Bay. Bull Fac Fish
791 Hokkaido Univ 31:84–114 (in Japanese with English abstract).
792 http://hdl.handle.net/2115/23707
793 Onishi H., Ooki A., Nomura D., Serizawa J., Amano K., and Okada M. (2017) Benthic
794 resources and fisheries environments in Funka bay (1), Annual report of Hokusui
795 Society Foundation in 2016, 77-88, *in Japanese*.

796 Ooki A, Yokouchi Y (2011a) Dichloromethane in the Indian Ocean: Evidence for in-situ
797 production in seawater, Mar. Chem., 124, 119–124, doi:
798 10.1016/j.marchem.2011.01.001
799 Ooki A., Yokouchi, Y (2011b) Determination of Henry's law constant of halocarbons in
800 seawater and analysis of sea-to-air flux of iodoethane (C_2H_5I) in the Indian and
801 Southern oceans based on partial pressure measurements. Geochem. J., 45, E1–E7
802 Ooki A, Nomura D, Nishino S, Kikuchi T, Yokouchi Y (2015) A global-scale map of
803 isoprene and volatile organic iodine in surface seawater of the Arctic, Northwest
804 Pacific, Indian, and Southern Oceans. J Geophys Res 120(6):4108–4128.
805 doi:10.1002/2014JC010519
806 Ooki A, Kawasaki S, Kuma K, Nishino S, Kikuchi T (2015b) Concentration maxima of
807 volatile organic iodine compounds in the bottom layer water and the cold, dense
808 water over the Chukchi Sea in the western Arctic Ocean: a possibility of production
809 related to degradation of organic matter. Biogeosciences Discussion, 12,
810 11245-11278, doi:10.5194/bgd-12-11245-2015
811 Palmer, PI, Shaw SL (2005) Quantifying global marine isoprene fluxes using MODIS
812 chlorophyll observations. Geophys Res Lett, 32(9) L09805, doi:
813 10.1029/2005GL022592
814 Price NM, Harrison GI, Hering JG, Hudson RJ, Nirel PMV, Palenik B, Morel FMM
815 (1989) Preparation and Chemistry of the Artificial Algal Culture Medium. Aquil Biol
816 Oceanogr 6(5–6):443–461. doi: 10.1080/01965581.1988.10749544
817 Sanadze GA (2004) Biogenic Isoprene (A Review). Russian J. Plant Physiol., 51(6)
818 729-741
819 Seebah S, Fairfield C, Ullrich MS, Passow U (2014) Aggregation and sedimentation of
820 *Thalassiosira weissflogii* (diatom) in a warmer and more acidified future ocean.
821 PLOS ONE 9(11):e112379. doi:10.1371/journal.pone.0112379

822 Shaw SL, Chisholm SW, Prinn RG (2003) Isoprene production by Prochlorococcus, a
823 marine cyanobacterium, and other phytoplankton. Mar Chem, 80:227–245. doi:
824 10.1016/S0304-4203(02)00101-9
825 Shaw SL, Gantt B, Meskhidze N (2010) Production and emissions of marine isoprene
826 and monoterpenes: a review. Advan Meteor 408696. doi:10.1155/2010/408696
827 Shimizu Y, Ooki A, Onishi H, Takatsu T, Tanaka S, Inagaki Y, Suzuki K, Kobayashi N,
828 Kamei Y, Kuma K (2017) Seasonal variation of volatile organic iodine compounds
829 in the water column of Funka Bay, Hokkaido, Japan. J Atmos Chem 74(2):205–225.
830 doi:10.1007/s10874-016-9352-6
831 Shinada A, Shiga N, Ban S (1999) Structure and magnitude of diatom spring bloom in
832 Funka Bay, southwestern Hokkaido, Japan, as influenced by the intrusion of Coastal
833 Oyashio Water. Plankton Biol Ecol 46(1):24–29
834 Stonner C, Edtbauer A, Williams J (2017) Real-world volatile organic compound
835 emission rate from seated adults and children for use in indoor air studies. Indoor air
836 28:164–172. doi:10.1111/ina.12405
837 Wang CM, Barratt B, Carslaw N, Doutsi A, Dunmore RE, Ward MW, Lewis AC (2017)
838 Unexpectedly high concentrations of monoterpenes in a study of UK homes.
839 Environ Sci Processes Impacts 19:528–537. doi:10.1039/c6em00569a
840 Wanninkhof, R. (1992) Relationship Between Wind-Speed and Gas-Exchange Over the
841 Ocean. J. Geophys. Res., 97, 7373-7382.
842 Welshmeyer NA (1994) Fluorometric analysis of chlorophyll a in the presence of
843 chlorophyll b and pheopigments, . Limnol. Oceanogr., 39, :1985–1992. doi:
844 10.4319/lo.1994.39.8.1985.
845 Yamaoka, H., Takatsu, T., Suzuki, K., Kobayashi, N., Ooki, and Nakaya, M. (submitted)
846 Annual and seasonal changes in the assemblage of planktonic copepods and
847 appendicularians in Funka Bay before and after intrusion of Coastal Oyashio Water
848 Assemblage of copepods and appendicularians. Fisheries Science.

849 Table 1 Temperature and salinity ranges of
850 uniform water masses in Funka Bay, Japan

	Temp. (°C)	Salinity
Tsugaru (T) water	8–15 °C	33.6–34.2
Winter (W) water	–1 to 5 °C	33.25–34.2
Oyashio (O) water	–1 to 10 °C[a]	32.6–33.0
Summer (S) water	10–25 °C	30.0–32.25

851 [a]Temperature range of Oyashio water was expanded from
852 the original definition (–1 to 2.5 °C; Ohtani and Kido 1980).

853

854

Table 2 Settings of C_5H_8 production rate calculation

	ΔC_{C5H8}	$F_{sea\text{-}air}$	[chl-a]	T
$P_{Mar(0–35m)}$	$[C_{C5H8}]_{(0\text{-}35\ m)}$ on 22 Mar - $[C_{C5H8}]_{(0\text{-}35\ m)}$ on 5 Feb (*)	Time-integrated sea-air flux (**)	Time-integrated average of $[chl\text{-}a]_{(0\text{-}35m)}$ amount from 25 Feb to 22 Mar (*)	26days; from 25 Feb to 22 Mar
$P_{Aug(20–40m)}$	$[C_{C5H8}]_{(20\text{-}40\ m)}$ on 29 Jul - $[C_{C5H8}]_{(20\text{-}40\ m)}$ on 27 Aug		Mean of $[chl\text{-}a]_{(20\text{-}40m)}$ on 29 Jul and 27 Aug	29days; from 29 Jul to 27 Aug
$P_{Mar(80–95m)}$	$[C_{C5H8}]_{(80\text{-}95\ m)}$ on 13 Apr - $[C_{C5H8}]_{(80\text{-}95\ m)}$ on 22 Mar		Mean of $[chl\text{-}a]_{(80\text{-}95m)}$ on 22 Mar	6 – 21 days (***)

(*) Values of concentration change of C_5H_8 and chl-a amount were multiplied by the depth range of 35 m in accordance with the unit of $F_{sea\text{-}air}$.

(**) $K\cdot([C_5H_8] - p\,C_5H_{8air}\cdot H)$; $K = 0.31\times u^2(Sc/660)^{-0.5}$ (*Wanninkhof*, 1992), where u is hourly wind speed obtained from the Muroran meteorological weather station, and Sc is Schmitt number. H: Henry's law constant of C_5H_8 in seawater (Ooki and Yokouchi, 2011), $[C_5H_8]$: mean concentration of C_5H_8 in the surface water on 5 February and 22 March, pC_5H_{8air}: partial pressure of C_5H_8 (80 patm). Mean flux obtained from the hourly flux was used for the production rate calculation.

(***) 6 days from 22 March to 27 March, and 22 days from 22 March to 13 April.

Figure captions

Fig. 1 Map showing the location of observation stations 30 and 23 in Funka Bay, Hokkaido, Japan, and Muroran, site of weather observations. Observation at the station 23 was additionally conducted in May 2018.

Fig. 2 Schematic diagram of incubation experiments and sample gas collection (upper panel), and calculation method of isoprene production rate (lower panel).

Fig. 3 Temperature–salinity ranges of water masses in Funka Bay, Japan

Fig. 4 Vertical profiles of temperature and salinity at station 30 in Funka Bay, Japan. Upper panels are December 2015 and February 2016, middle panels are March–May 2016, and lower panels are July–November 2016. The light-gray profiles in the middle and lower panels are the last profiles from the upper and middle panels, respectively, copied for comparison. W, winter water; O, Oyashio water

Fig. 5 Seasonal trend of water-mass structure at station 30 in Funka Bay, Japan. The four main water masses are Tsugaru water (T), winter water (W), Oyashio water (O), and summer water (S). Transition waters are WO, WOT, ST, TW and OS. Depth ranges and periods for estimations of isoprene production rates ($P_{Mar(0\text{-}35m)}$, P_{Bottom}, and $P_{Aug(20\text{-}40m)}$) were enclosed by bold broken line.

Fig. 6a Vertical profiles of isoprene (C_5H_8), apparent oxygen utilization (AOU), dissolved inorganic nitrogen (DIN), and chlorophyll-a (chl-a) in December 2015–February 2016 (upper panels) and March–April 2016 (lower panels) at station 30 in Funka Bay, Japan. The x-axis of chl-a in March and April was decupled with the

891 labeled value.

892

893 Fig. 6b Vertical profiles of isoprene (C_5H_8), apparent oxygen utilization (AOU),
894 dissolved inorganic nitrogen (DIN), and chlorophyll-a (chl-a) in May 2016 (upper
895 panels) and July–November 2016 (lower panels) at station 30 in Funka Bay, Japan

896

897 Fig. 7 Vertical profiles of photosynthetically active radiation (PAR) in 2016 at station
898 30 in Funka Bay, Japan. The depths of 0.5% of surface PAR are marked by arrows. The
899 data for April were measured on 14 April at another station in Funka Bay. Weather
900 conditions on 14 April were cloudy

901

902 Fig. 8 Changes in isoprene concentrations in the surface mixed layer from 5 February to
903 22 March 2016

904

905 Fig.9 Interpolation of surface chl-a concentrations on 25 February and 8 March from the
906 fluorescence monitoring data. 'Obs.' is the chl-a concentration measured by
907 Welshmeyer method (this study), 'Fluor.' is the chl-a concentration measured by
908 fluorometer (surface monitoring data by Yamaoka et al. (*submitted*)), and 'Cal.' is the
909 interpolated calibration data of chl-a concentration.

910

911 Fig. 10 Results of incubation experiment I. Shaded and white areas indicate the
912 exponential growth phase (i), steady phase (ii), decline phase (iii), and stagnation phase
913 (iv)

914

915 Fig. 11 Results of incubation experiment II. Shaded and white areas indicate the
916 exponential growth phase (i), steady phase (ii), decline phase (iii), and stagnation phase
917 (iv). Cultures were moved from 13-h:11-h (L:D) into continuous darkness on day 12

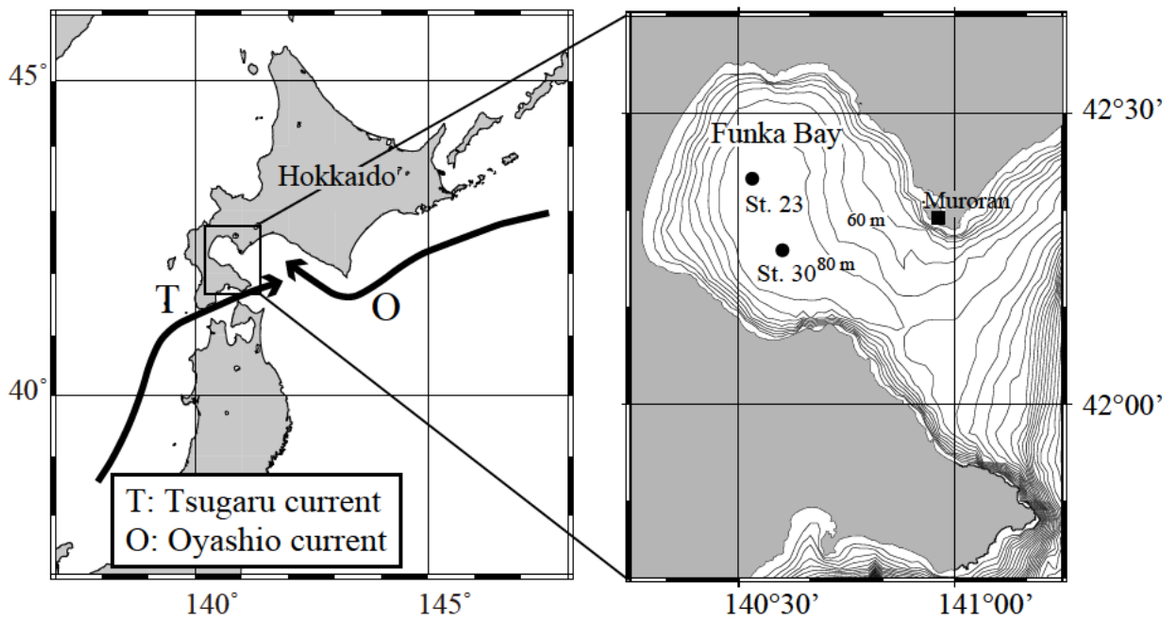
45˚
40˚
140˚
145˚
Hokkaido
T
O
T: Tsugaru current
O: Oyashio current
Funka Bay
St. 23
St. 30
60 m
80 m
Muroran
42°30’
42°00’
140°30’
141°00’

Figure 1

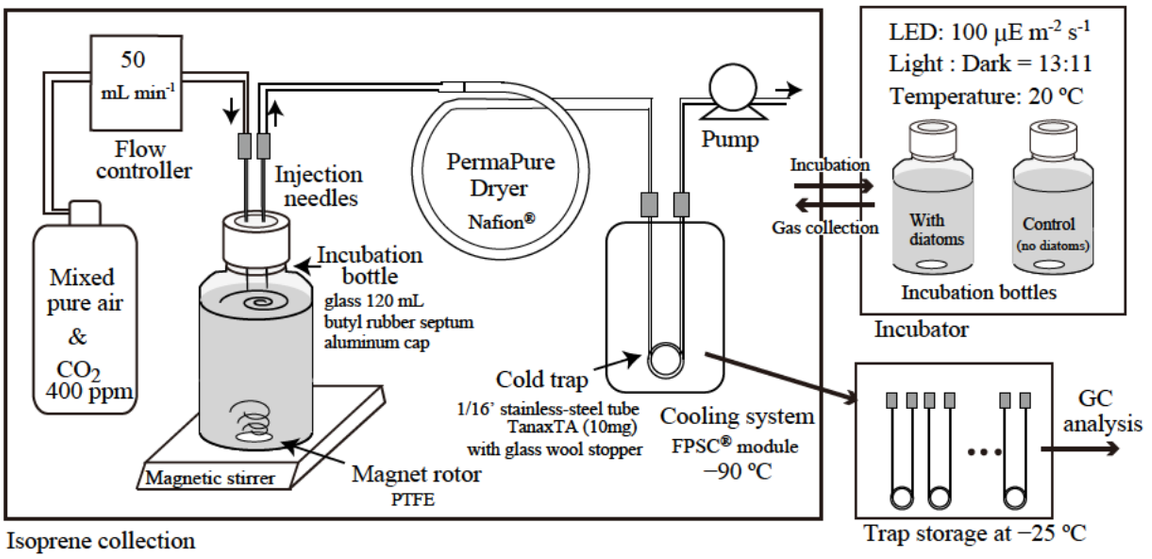

Isoprene collection

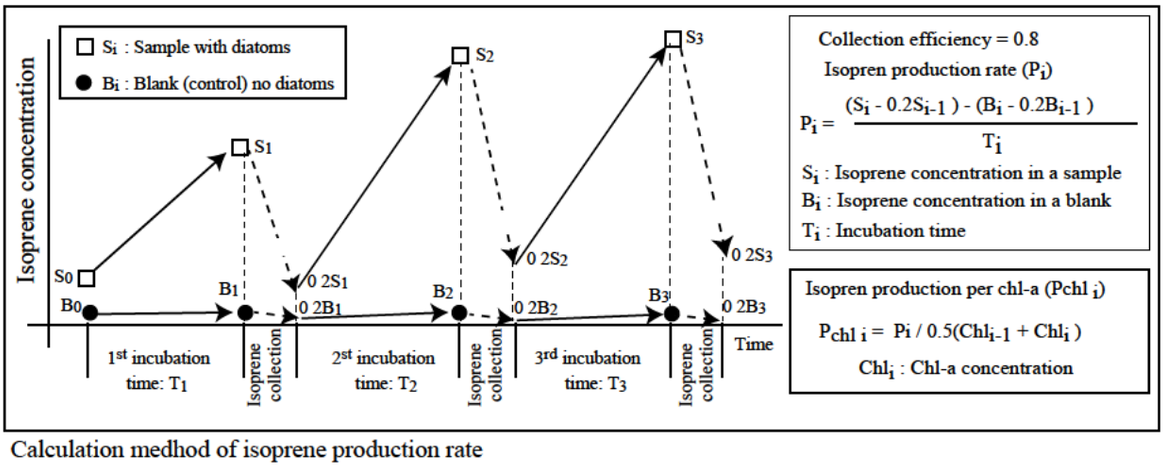

Calculation medhod of isoprene production rate

Figure 2

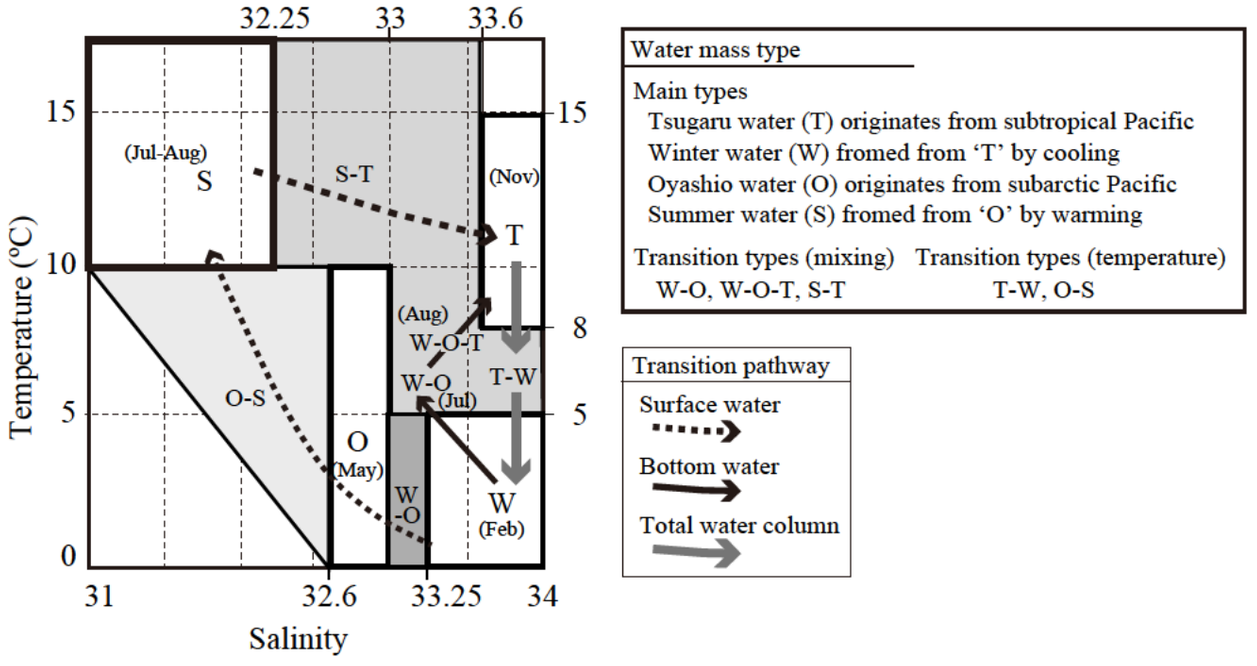
32.25
33
33.6
15
10
5
0
15
8
5
Temperature (°C)
31
32.6
33.25
34
Salinity
(Jul-Aug)
S
S-T
(Nov)
T
(Aug)
W-O-T
W-O
(Jul)
T-W
O-S
O
(May)
W
-O
W
(Feb)
Water mass type
Main types
Tsugaru water (T) originates from subtropical Pacific
Winter water (W) fromed from 'T' by cooling
Oyashio water (O) originates from subarctic Pacific
Summer water (S) fromed from 'O' by warming
Transition types (mixing)
W-O, W-O-T, S-T
Transition types (temperature)
T-W, O-S
Transition pathway
Surface water
Bottom water
Total water column

Figure 3

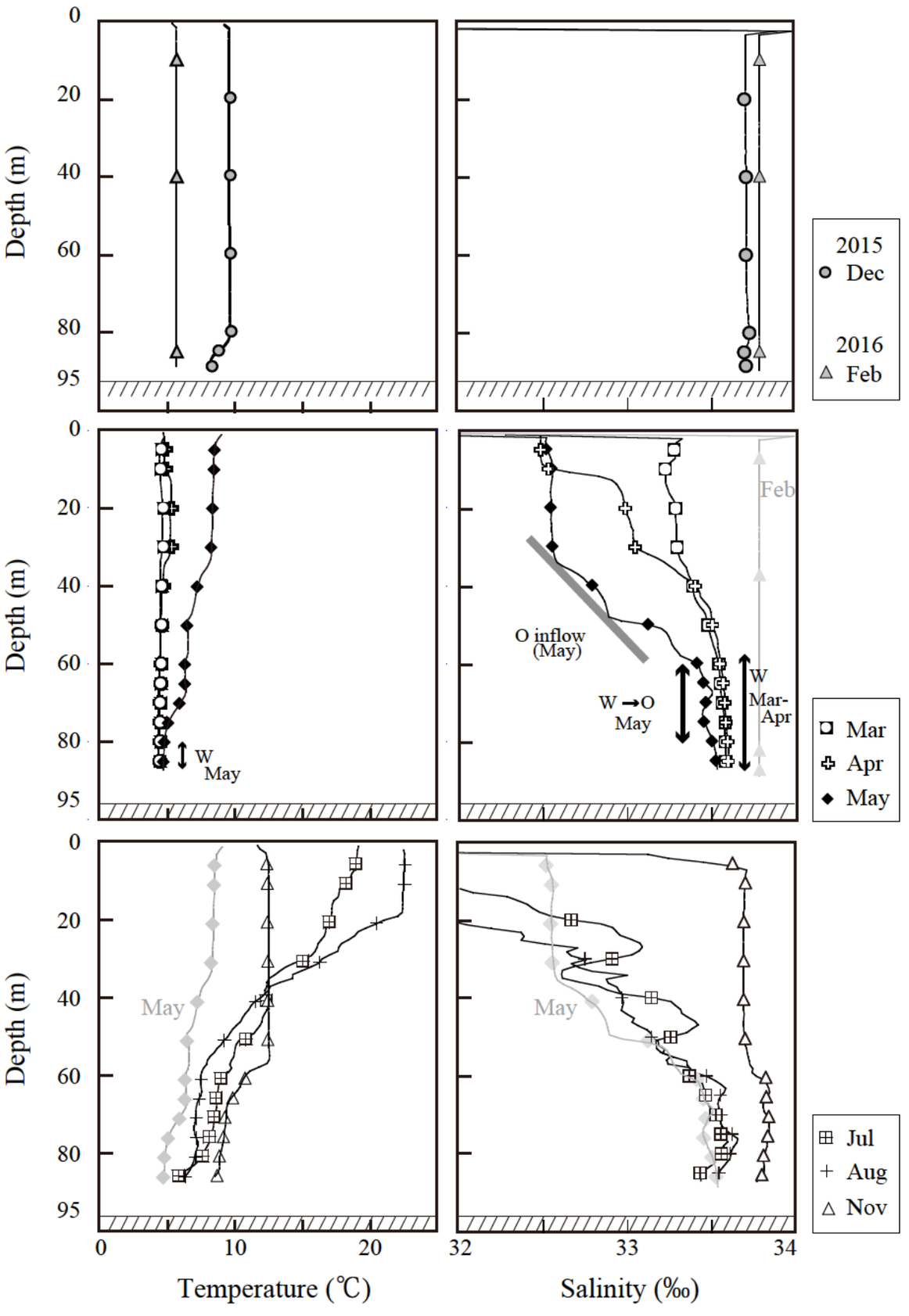
Depth (m)
0
20
40
60
80
95
2015
Dec
2016
Feb
W
May
O inflow
(May)
W→O
May
W
Mar-
Apr
Feb
Mar
Apr
May
May
Jul
Aug
Nov
0
10
20
32
33
34
Temperature (℃)
Salinity (‰)

Figure 4

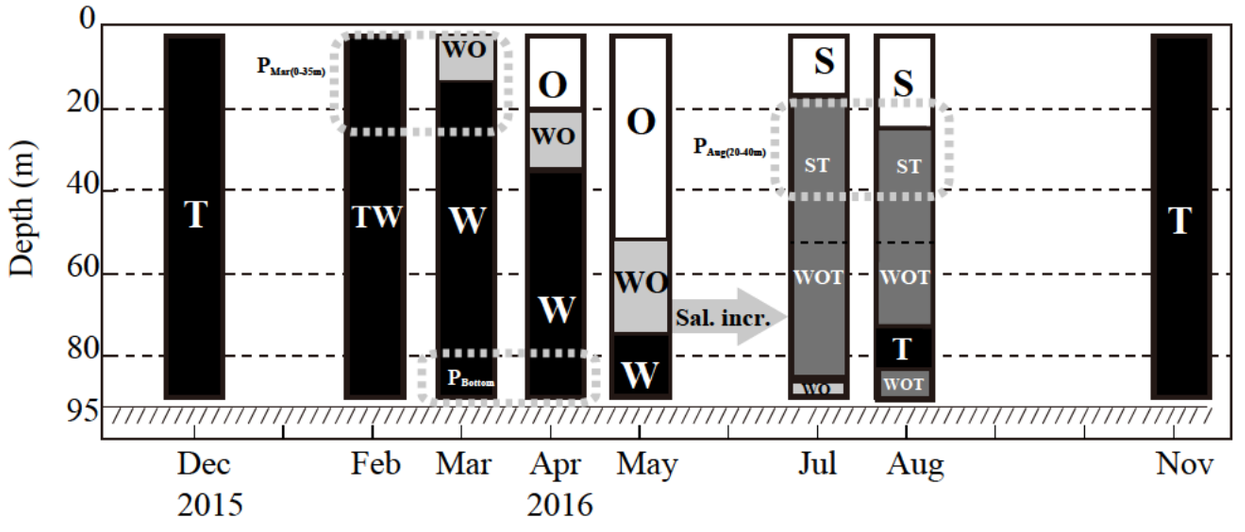
0
20
40
60
80
95
Depth (m)
T
TW
W
WO
O
WO
W
O
WO
W
S
ST
WOT
WO
S
ST
WOT
T
WOT
T
P Mar(0-35m)
P Bottom
P Aug(20-40m)
Sal. incr.
Dec
2015
Feb
Mar
Apr
2016
May
Jul
Aug
Nov

Figure 5

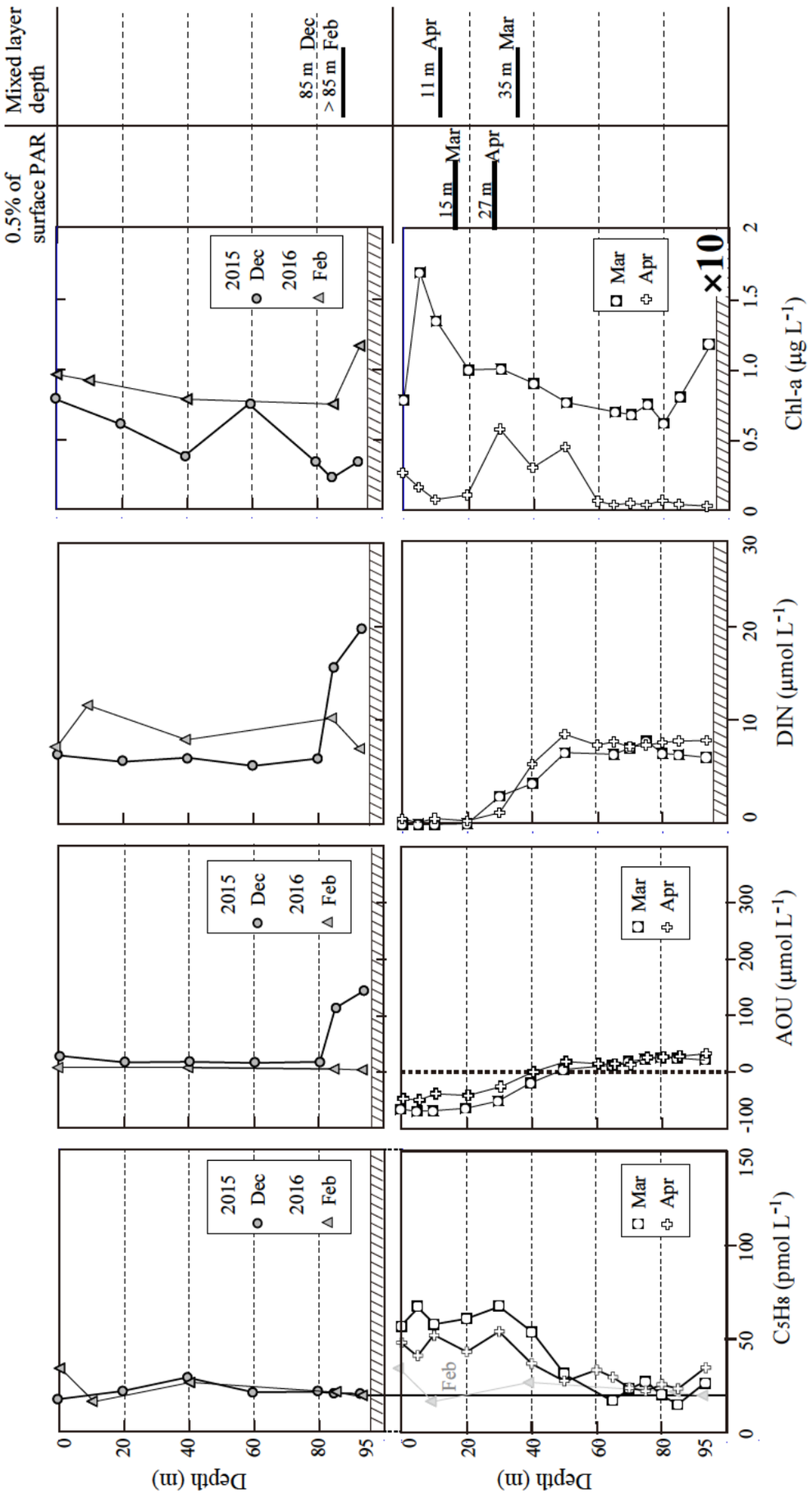
Mixed layer depth
0.5% of surface PAR
85 m Dec
> 85 m Feb
11 m Apr
15 m Mar
27 m Apr
35 m Mar
2015 Dec 2016 Feb
Mar Apr
×10
Chl-a (µg L-1)
DIN (µmol L-1)
AOU (µmol L-1)
C5H8 (pmol L-1)
Feb
Depth (m)

Figure 6a

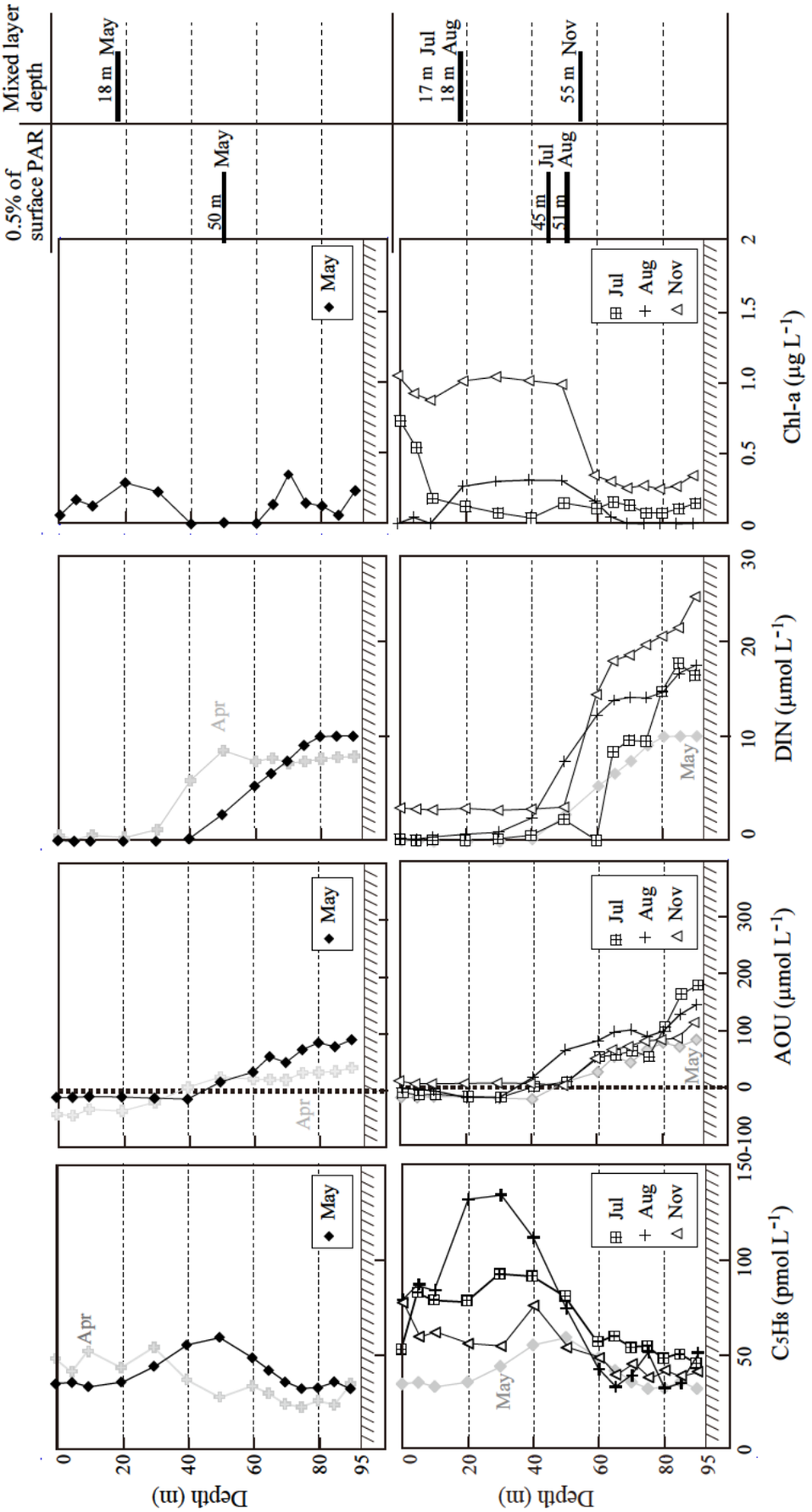
Mixed layer depth
0.5% of surface PAR
18 m May
50 m May
17 m Jul
18 m Aug
45 m Jul
51 m Aug
55 m Nov
May
Apr
Jul
Aug
Nov
Depth (m)
C5H8 (pmol L-1)
AOU (µmol L-1)
DIN (µmol L-1)
Chl-a (µg L-1)

Figure 6b

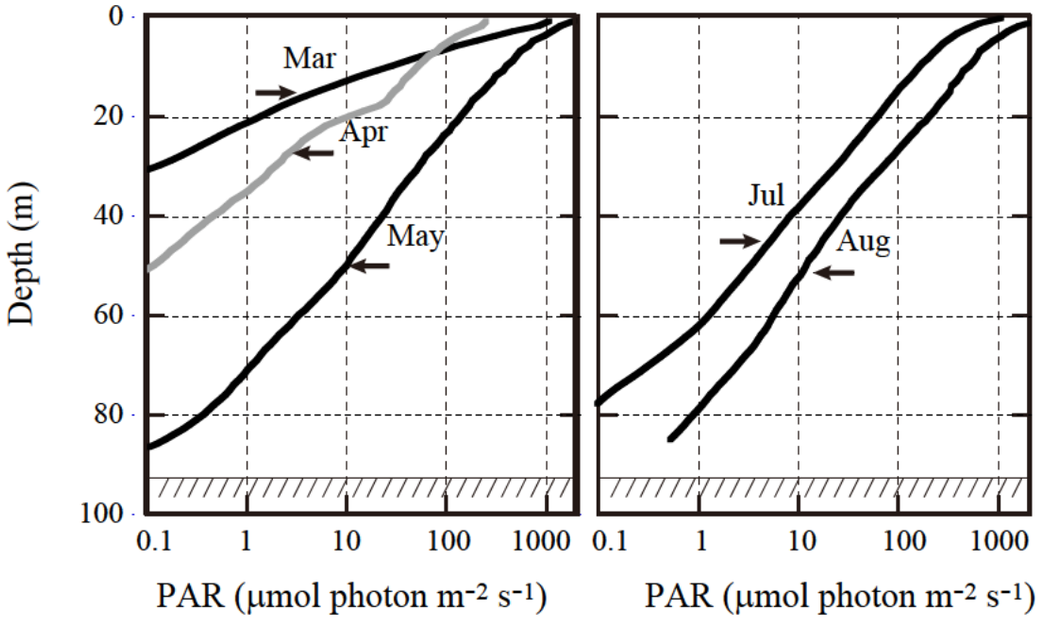
0
20
40
60
80
100
Depth (m)
Mar
Apr
May
Jul
Aug
0.1
1
10
100
1000
PAR (µmol photon m-2 s-1)
PAR (µmol photon m-2 s-1)

Figure 7

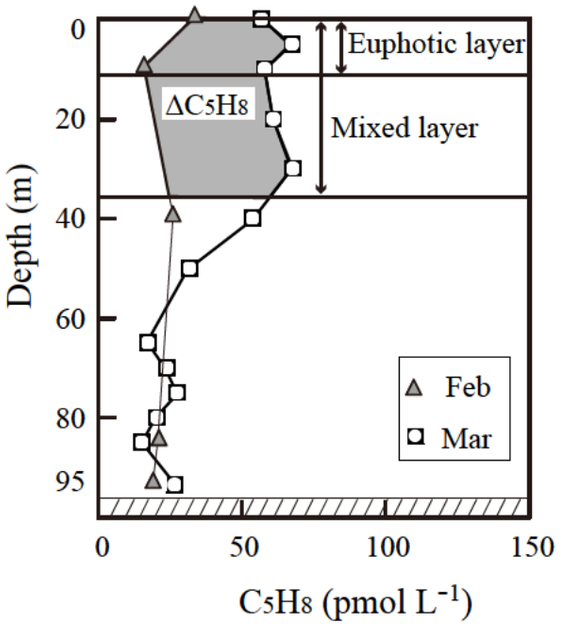
0
20
40
60
80
95
Depth (m)
Euphotic layer
Mixed layer
ΔC5H8
Feb
Mar
0
50
100
150
C5H8 (pmol L-1)

Figure 8

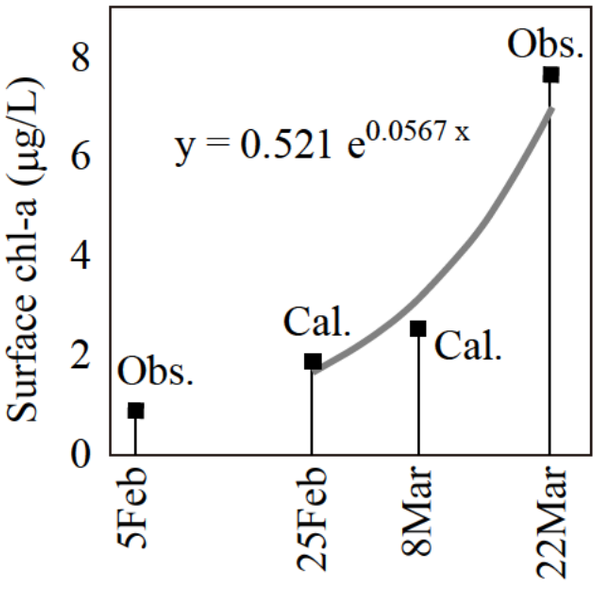

Surface chl-a conc. (µg/L)

	Obs.	Fluor.	Cal.
5Feb	0.95	0.27	
25Feb		0.41	1.92
8Mar		0.51	2.62
22Mar	7.75	1.25	

[Cal] = 6.94 [Fluor] - 0.92

Figure 9

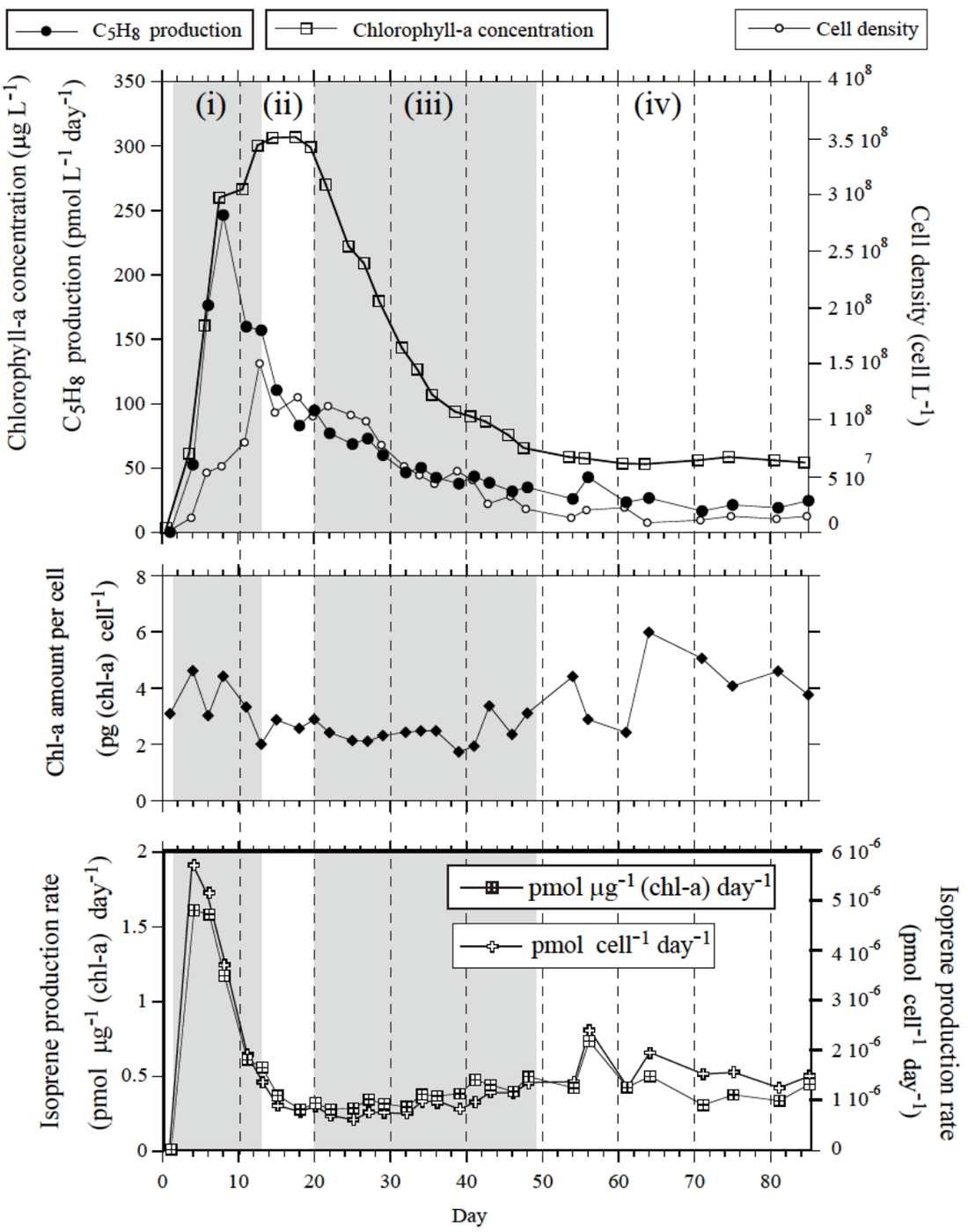
C5H8 production
Chlorophyll-a concentration
Cell density
Chlorophyll-a concentration (μg L-1)
C5H8 production (pmol L-1 day-1)
Cell density (cell L-1)
(i)
(ii)
(iii)
(iv)
Chl-a amount per cell
(pg (chl-a) cell-1)
Isoprene production rate
(pmol μg-1 (chl-a) day-1)
pmol μg-1 (chl-a) day-1
pmol cell-1 day-1
Isoprene production rate
(pmol cell-1 day-1)
Day

Figure 10

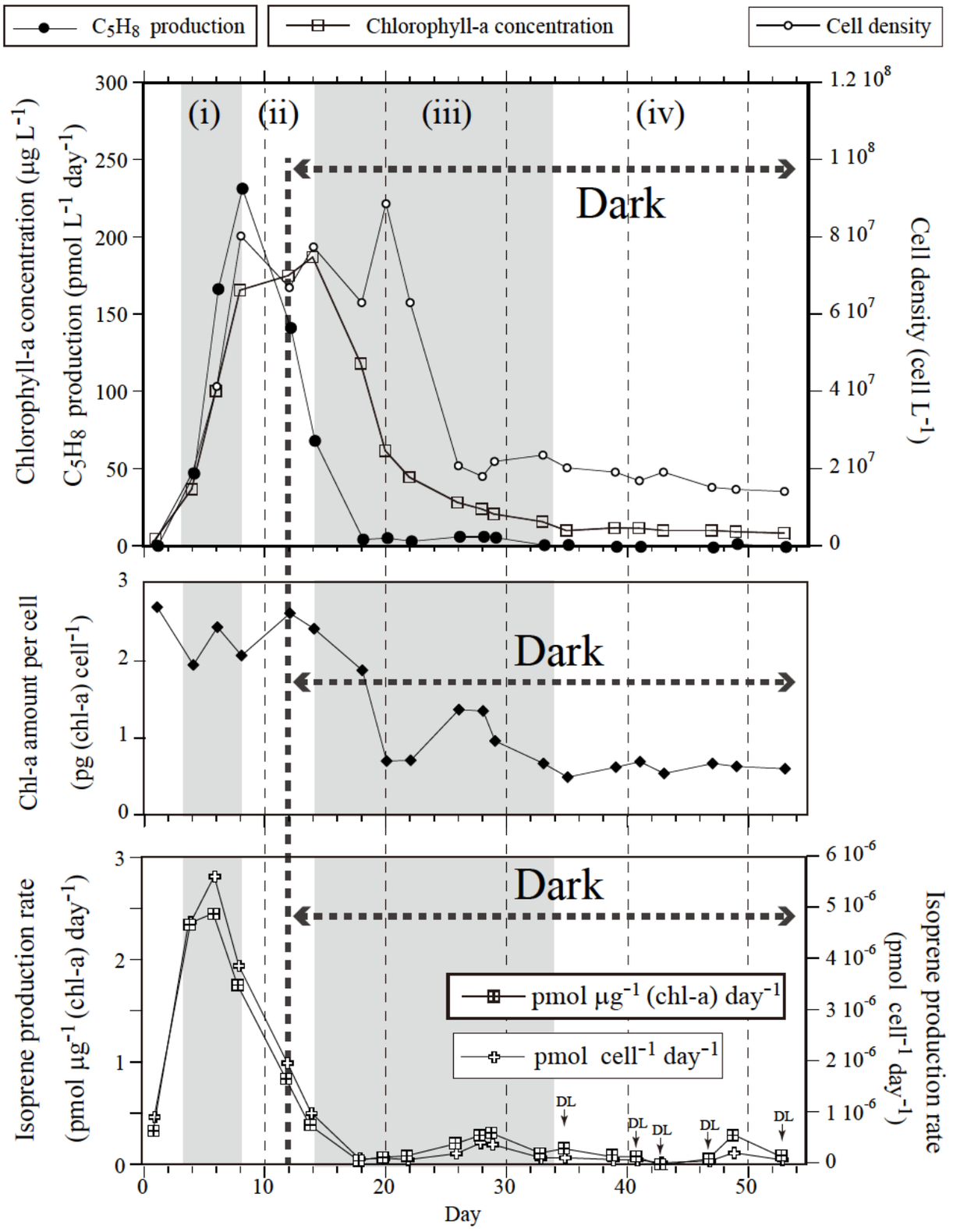
C5H8 production
Chlorophyll-a concentration
Cell density
(i)
(ii)
(iii)
(iv)
Dark
Chlorophyll-a concentration (μg L-1)
C5H8 production (pmol L-1 day-1)
Cell density (cell L-1)
Chl-a amount per cell
(pg (chl-a) cell-1)
Isoprene production rate
(pmol μg-1 (chl-a) day-1)
Isoprene production rate
(pmol cell-1 day-1)
pmol μg-1 (chl-a) day-1
pmol cell-1 day-1
DL
Day

Figure 11